Applied Catalysis B: Environmental 259 (2019) 118050

Contents lists available at ScienceDirect

Applied Catalysis B: Environmental

journal homepage: www.elsevier.com/locate/apcatb

Highly dispersed platinum supported catalysts – Effect of properties on the electrocatalytic activity

Eirini Zagoraiou[a], Maria K. Daletou[a,*], Labrini Sygellou[a], Stella Ballomenou[b], Stylianos G. Neophytides[a]

[a] Foundation of Research and Technology, Hellas - Institute of Chemical Engineering Sciences, FORTH/ICEHT, Stadiou Str, Platani Rion, P.O. Box 1414, Patras GR-26504, Greece

[b] Chemical Process & Energy Resources Institute - Centre for Research & Technology-Hellas, CPERI/CERTH, 6th km Charilaou-Thermi Road, 57001 Thessaloniki, Greece

ARTICLE INFO

Keywords:
Platinum deposition
Functionalized nanotubes
High/atomic dispersion
Oxygen reduction reaction
Electrochemical activity

ABSTRACT

This work addresses scientific issues regarding the most challenging component of PEM fuel cells, the electrocatalyst, and explores a new approach to exploit the differentiations induced to the metal by the surface chemistry of the support. The study focuses on the development of Pt based electrocatalysts supported on pyridine modified carbon nanotubes with different Pt loadings, their thorough characterization and parallel comparison with non-modified or conventional carbon supports. The aim is the interpretation of the catalyst electrochemical behavior through a structural and physicochemical characterization study. The introduction of pyridines can differentiate the metal deposition, in terms of dispersion, nanoparticle properties, platinum oxidation state and metal-support interactions. Moreover, the substrate can play a decisive role on the size and functionality of the electrochemical interface. This approach constitutes a promising route for developing materials with innovative features aiming to a serious reduction in the Pt loads through increased activity and metal utilization.

1. Introduction

Hydrogen combined with fuel cell technologies can provide green energy and reduced greenhouse gas emissions originating from fossil fuel utilization. The route towards a sustainable energy economy involves the efficient development of fuel cells. In particular, many efforts have been devoted to improve the performance of Polymer Electrolyte Fuel Cells (PEMFCs) and minimize their overall cost. PEMFCs are considered as the ideal clean power source and an attractive candidate for many applications because of their high power density, high efficiency, constructive simplicity, quick start-up and zero emission [1,2]. The heart of the fuel cell technology practically consists of a polymer electrolyte sandwiched between two Pt based electrodes.

One of the most decisive operating parameters is their working temperature. Low temperature PEMFCs are in general electrochemically more efficient when operating on pure H_2, thus being mainly applicable in automotive applications. High temperature PEMFC system offers advantages including a number of fueling options, the simplifications of the balance of plant and the generation of more useful high-grade waste heat, making them more promising candidates for stationary applications. In both cases, Pt supported on carbon electrocatalysts are the most efficient and stable materials for both the Oxygen Reduction Reaction (ORR) at the cathode and the Hydrogen Oxidation Reaction (HOR) at the anode in PEMFCs. Due to the sluggish kinetics of the ORR [3,4], and poor stability particularly at the oxygen electrode, a high Pt loading is normally required to maintain the desirable cell performance, resulting in high cost of PEMFCs, thus hindering their commercialization [5]. What is even more significant is that most of the Pt amount on the electrodes is not efficiently used. Only the particles that are in contact with the electron conductor (carbon), the proton conductor (electrolyte) and the reacting gases are electrochemically active. Forming an extended and stable interface and fully utilizing Pt is a challenging task. Even in the state of the art electrode formulations, the percentage of the surface area that is electrochemically active is low compared to the total amount of the catalyst used. In this respect, reduced cost resulting from increased catalyst activity and/or utilization is highly desirable [6] and the most challenging areas towards the optimization of this technology is the development of catalytic layers with structures and architectures that lead to more active and extended electrochemical interfaces with minimal Pt loads.

One approach to achieve this reduction is to enhance the specific

* Corresponding author.
E-mail address: riadal@iceht.forth.gr (M.K. Daletou).

https://doi.org/10.1016/j.apcatb.2019.118050
Received 25 February 2019; Received in revised form 29 July 2019; Accepted 3 August 2019
Available online 08 August 2019
0926-3373/ © 2019 Elsevier B.V. All rights reserved.

activity by using additives or co-catalysts and/or by influencing the electronic properties of the catalyst. Most commonly addressed route is the formation of alloys with Co and Ni, which are extensively studied materials with certain advances and limitations. An effective catalyst must be reaction specific and its interaction with intermediates should be neither too strong nor too weak. If the interaction is too weak, the intermediate will fail to bind to the catalyst and no reaction will take place. On the other hand, if the interaction is too strong, the catalyst gets blocked by the intermediate and further catalytic reactions are impeded [7]. The above can be modified and possibly controlled by triggering changes on both electronic (ligand) and geometric (strain) catalyst properties [8].

Increase of the specific surface area of the catalyst by forming a fine dispersion can be achieved by altering/modifying the high surface area support and/or optimizing the metal deposition method so that an effective anchoring of the metal nanoparticles can be achieved. When the dispersion of the metal is high, there are many active metal atoms on a surface. Reducing the size to small metal particles or even atoms could significantly increase both the active surface and the catalyst activity through diversification or strengthening of the metal-support interactions [9]. However, it is very difficult to achieve high and/or atomic dispersion, as well as to maintain the morphology under reaction conditions, since the atoms or few atom small particles tend to agglomerate.

The nature of the effect of the carrier on the electronic and catalytic properties of supported metal catalysts is very important. The support acts as a supramolecular ligand and has been claimed to promote specific electronic properties and/or geometrical features of the nano-sized supported metal particles. It is well reported that the interaction between Pt and carbon support (metal support interaction) [10], as well as the interaction of Pt precursor with carbon during the supported catalyst formation, in terms of electronic structure change, are considered to be beneficial to the improvement of electrocatalytic activity and durability of the electrocatalysts [11,12]. Moreover, it is well established that the reaction rates of the ORR on Pt(hkl) surfaces are structure sensitive, i.e. their electrochemical reactivity and selectivity depend on the local symmetry of the catalytically active Pt atoms and are greatly influenced by the structural sensitivity of the adsorption of spectator species like anions from the supporting electrolyte [13–16]. This is induced by the structure sensitive inhibiting effect of OH_{ads} species on Pt facets that block active sites for O_2 adsorption and retard ORR kinetics [4,5,17–19].

Furthermore, there are many and often contradictory results on the particle size effect on the kinetics of ORR. Even though smaller platinum particles (< 2 nm) is believed to be less active for the ORR (due to stronger Pt-O binding on them) [20], many studies reported that much smaller particles (clusters) showed better ORR performance [21]. Although substantial efforts have been devoted in the last decades to study the crystal planes and size effect on the ORR activity, few studies have investigated and concluded on the influence of the Pt particle distribution, the interparticle distance and the metal-support interactions. Moreover, there are even fewer attempts to reach a high level of understanding on these phenomena, in order to be able to make targeted modifications to the electrocatalyst, alter its properties and tune the ORR activity and selectivity.

High or atomic dispersion of supported metals is most commonly addressed on oxide supports like ceria, alumina, silica etc or other supports with many defects, in order to obtain atomic or subnanometer oxidized clusters that are strongly bound through interactions with the support [9,22–32]. Mononuclear ensembles consisting of cationic metals anchored to supports through M–O linkages have been formed and stabilized on supports in configurations that are stable and active for several reactions. In most cases, the targeted applications include redox reactions like oxidation of CO and of hydrocarbons, as well as the Water-Gas Shift (WGS) reaction [33,34]. The main advantage of this dispersion is that each metal atom which is accessible to reactants is available for catalysis, maximizing the efficiency of the precious metal use and minimizing the cost. Furthermore, reducing the size can bring drastic changes in the properties [9,35]. Proposed reaction mechanisms for the aforementioned reactions involve cationic metal species, as well as invoking synergistic effect from the support, acting as a structure stabilizer and an oxygen reservoir [36]. Nevertheless, the exact mechanistic scheme that would allow controlling the selectivity and catalytic activity remains unclear even for these thoroughly studied reactions.

Unfortunately, metal oxide supports are generally insulators or semiconductors and unstable under corrosive electrochemical operating conditions [37]. Carbon based materials with good electron conductivity and stability are ideal candidates for supports in electrocatalysis. Nevertheless it is rather challenging to stabilize metal clusters even of a few nanometers on carbon surfaces [38–42]. Even more, it is difficult to distinguish mononuclear metal complexes from small metal clusters, identify the catalytic species, understand the modifications on the electronic surface state of the metal and exploit all the above in order to tune the (electro)catalytic properties.

Carbon nanotubes [43,44], single (SWCNTs) or multi (MWCNTs) walled, appear to be promising candidates for use as support materials in fuel cells [45–50], due to their high specific surface area [51], good thermal, chemical and mechanical stability as well as high electrical conductivity. Usually carbon nanotubes with increased amount of functional groups after oxidative treatment are used [45,52], to assist fine dispersion of Pt. Orfanidi et al [53] reported that surface modification of MWCNTs with pyridines significantly affects the dispersion of Pt particles, either by providing anchoring sites for Pt ions from the Pt precursor or improving the wetting of the support with the reaction solution. The reason for this specific functionalization lies in the nature of the polymer electrolyte used in such cells, which is doped with phosphoric acid in order to conduct protons [54]. Pyridine groups are able to interact with phosphoric acid [55] achieving increased contact of the active phase (Pt) with the proton conductor and thus the extension and stabilization (even under harsh reformate conditions) of the electrochemical interface and the increase of the catalyst utilization [56].

In the present work the study is focused on the development of Pt electrocatalysts supported on pyridine functionalized oxidized MWCNTs, Pt/(ox.MWCNT)-Py, with different Pt loadings and their physicochemical characterization. The introduction of pyridines on the sidewalls of the carbon support is expected to differentiate the deposition of Pt, not only in terms of dispersion, but also with respect to metal-support interactions, platinum crystal properties and/or oxidation state. The aim of this work is the interpretation of the catalyst electrochemical behaviour through a structural and chemical characterization study. This in depth knowledge will leverage the level of understanding and finally will allow to tune the selectivity and activity of the metal supported catalysts on carbon supports.

2. Experimental section

Preparation of carbon nanotube supports. High purity Multi-Wall Carbon Nanotubes, MWCNT, 97% of diameter ranging between 10 and 30 nm were purchased from Nanothinx S.A. The oxidation of MWCNT with nitric acid (65 wt%) for 48 h resulting in ox.MWCNT, as well as their subsequent functionalization with pyridine groups using the solvent-free functionalization method with 3-aminopyridine and isoamyl nitrate resulting in (ox.MWCNT)-Py, took place according to already published procedures [53]. The successful functionalization was confirmed via thermal gravimetric analysis (TGA), Raman and X-ray Photoelectron Spectroscopy (XPS) [52].

Synthesis of Pt based catalysts. All the catalysts were synthesized via an already optimized procedure [53]. Dihydrogen hexachloroplatinate (IV) hexahydrate (99.95% metals basis, Alfa Aesar) was dissolved in water resulting in a 0.25 M solution and was used as the platinum

precursor. The amount of the precursor was calculated in order to obtain a final 1, 2, 3, 4, 5, 10, 15 or 30 wt% Pt catalyst loading with respect to the MWCNTs. An example of the experimental procedure followed is given below for the Pt based electrocatalyst on ox.MWCNT with 10 wt% Pt loading: In a round bottom flask, 150 mg of ox.MWCNT were dispersed in 300 ml of an ethylene glycol (EG)/H_2O 3/1 (v/v) mixture. 0.342 ml of the hexachloroplatinic acid solution was added and the reaction mixture was left stirring for 17 h at RT. Thereafter, the reduction reaction was performed under reflux conditions at 120 °C for 2 h. The catalyst was obtained by filtration, washed with milli-Q water and dried overnight at 70 °C under vacuum.

Synthesis of unsupported Pt nanoparticles in the presence of Py in the reaction solution. 33 μl of pyridine (99.6%, RPE-ACS, Carlo Erba) were added in 200 ml of an EG/H_2O 3/1 (v/v) mixture and the solution was left under stirring for 75 min. Subsequently, 2 ml of the 0.25 M aqueous hexachloroplatinic acid solution were added and the solution was left stirring for 18 h at RT. Thereafter, the reduction reaction was performed under reflux conditions at 120 °C for 2 h. The unsupported nanoparticles were obtained by filtration, washed with milli-Q water and dried overnight at 70 °C under vacuum.

"Deposition" of platinum precursor ions on nanotubes with no reduction reaction. In a round bottom flask, 40 mg of ox.MWCNT or (ox.MWCNT)-Py were dispersed in 40 ml of H_2O. 0.352 ml of the 0.25 M aqueous hexachloroplatinic acid solution were added and the solution was left under stirring for 19 h at RT. The amount of the precursor was calculated as to obtain a 30 wt% Pt loading. The solid was obtained by filtration, washed thoroughly with milli-Q water and dried overnight at 70 °C under vacuum.

The same deposition took place in the presence of Py in the solution in the case of (ox.MWCNT)-Py. The same experimental procedure was followed, but 3 h before the final filtration, 4.36 μl of pyridine were added in the solution.

Physical characterizations. The crystalline structure of the catalysts was analyzed via an X-ray powder diffractometer (Bruker D8 Advance) using Cu Kα radiation. The Powder XRD (*p*XRD) measurements were carried out in the 2θ angle with the range of 20–90 °.

The size, and dispersion of catalyst nanoparticles were characterized by transmission electron microscopy (TEM) on JEOL JEM2100 operating at 200 kV. Sample preparation involved the ultrasonic dispersion of the sample (1 min) in water and placing a drop of the suspension on carbon coated copper grids (dia. 3 mm, Electron Microscopy Sciences). The mean particle size was estimated by counting around 600 isolated particles in different TEM images. A small deviation from the actual size is probable, given the difficulty in identifying Pt particles in the clusters as depicted in the TEM images especially at high loadings and in the case of the ox.MWCNT substrate.

X-ray Photoelectron Spectroscopy (XPS) experiments of the CNT samples were carried out in a commercial ultrahigh vacuum system ($P < 10^{-9}$ mbar), which consists of a fast entry specimen assembly, a preparation, and an analysis chamber. The analysis chamber is equipped with a SPECS LHS-10 hemispherical electron analyzer and a twin-anode X-ray gun. The XPS measurements were performed at room temperature using non-monochromatized AlKα radiation, and a pass energy analyzer of 97 eV, giving a full-width-at-half-maximum FWHM of 1.7 eV for the Au $4f^{7/2}$ peak. The accuracy for BEs (Binding Energies) assignments is ˜0.1 eV. In all samples, the main C 1s peak was at 284.6 eV. The XPS core level spectra were analyzed with a fitting routine, which decomposes each spectrum into individual, mixed Gaussian–Lorentzian peaks using a Shirley background subtraction over the energy range of the fit, imposing a FWHM of 1.8 eV for metallic platinum and 2.1 eV for Pt oxides.

The elemental analysis for all catalysts was performed via Inductively Coupled Plasma – Optical Emission Spectrometer, ICP-OES (Perkin Elmer Optima 4300 Dual View model). 10–20 mg of each catalyst sample was dissolved into 2 ml hydrochloric acid and 2 ml nitric acid, while the extraction of the metals was done in a microwave under pressure of 120 psi for 20 min. Calibration curves, i.e. range at 0.1–100 mg/L were obtained using appropriate blank and standard solutions (dilutions from certified stock solution provided by CPAchem). The exact conditions of the ICP-OES measurement were:

- Plasma flow: 15 L/min
- Auxiliary flow: 0.2 L/min
- Nebulize flow: 0.6 L/min
- RF Power: 1300 watts
- Plasma View: radial view
- Sample Flow Rate: 2 ml/min

Electrochemical measurements. The experimental setup employed for the rotating disk electrode (RDE) experiments was based on a Princeton Applied Research MSR Rotator and an Autolab galvanostat–potentiostat PGSTAT-302. The catalysts were evaluated in a 100 ml solution of 0.1 M $HClO_4$ at room temperature using a typical three-electrode electrochemical cell employing a capped 150 ml glass cell, a Pt wire as the counter electrode, a sealed reference hydrogen electrode, RHE, and the rotating working electrode. The glassy carbon (GC) electrode disk (d = 0.5 cm) was purchased from Pine Instruments, Inc. Prior to the deposition of the catalyst ink, the rotating disk substrate was polished to a mirror finish (0.05 mm alumina, Buehler). The ink was prepared by ultrasonic suspension of 1.8 mg of catalyst into 5 ml milli-Q H_2O and 2-propanol 1/8 (v/v). A certain volume of the suspension was deposited on the glassy carbon disk via a micro-syringe and the disk was rotated (around 100 rpm) until the solvent was evaporated. The catalyst loading on the disk electrode was optimized using the 30 wt% Pt/(ox.MWCNT)-Py and following the calibration procedure reported by Mayrhofer et al 57. A series of measurements were carried out with metal loadings ranging from 10 μgPt/cm^2 to 30 μgPt/cm^2, corresponding to catalyst loadings onto the disk between 33 and 100 μg/cm^2, respectively. It was observed that within the range of 10 to 20 μgPt/cm^2, the theoretical diffusion limiting current was reached in all cases and very importantly the specific current at 0.9 V was constant. At higher catalyst loadings (> 67 μg/cm^2) and thus thicker catalytic layers, the specific current decreased indicating that, within the thicker catalytic layers, internal mass transfer resistance was prevailing, affecting the uniform access of the reacting O_2 gas to the Pt surface. In the present study several catalysts with different Pt loadings are tested. In order to get reliable measurements and avoid any mass transport limitations within the catalytic layer in the kinetic region, all samples have been prepared with the same catalyst layer thickness. This can be achieved by controlling the amount of catalyst that will be loaded on the disk so that the amount of the carbon support is maintained constant for all samples. According to the aforementioned calibration procedure, the optimum chosen catalyst loading on the glassy carbon for the 30 wt% Pt/(ox.MWCNT)-Py was 67 μg/cm^2, corresponding to a Pt loading of 20 μg/cm^2 and carbon support loading of 47 μg/cm^2. Thus, considering a variation of the Pt loading on the MWCNT support from 1 to 30 wt%, the corresponding loading of Pt on the electrode varies from 0.43 μg/cm^2 to 20 μg/cm^2.

As it will be discussed later (Fig. 7), for the low Pt loading catalysts (1–5 wt%), the recorded limiting current is lower than the theoretical limiting current observed for Pt loadings > 5 wt%. Further increase of the catalyst amount on the electrode (above 47 μg/cm^2 of carbon support) did not improve significantly the obtained limiting current for the 1–5 wt% samples, whereas the thicker formed layer introduced deviations from the specific activity at 0.9 V vs RHE. Ultrahigh purity grade gases Ar and O_2 were used. Saturation of the solution was achieved by bubbling the gas through the electrolyte for at least 30 min prior to measurements. Thereafter, measurements were carried out under a slight overpressure of Ar or O_2 above the solution level. The common procedure followed was (i) Cycling in Ar-saturated 0.1 M $HClO_4$ solution at sweep rates of 100 and 20 mV/s from 0.03 to 1.2 V. Active surface area was estimated from the surface of hydrogen under-

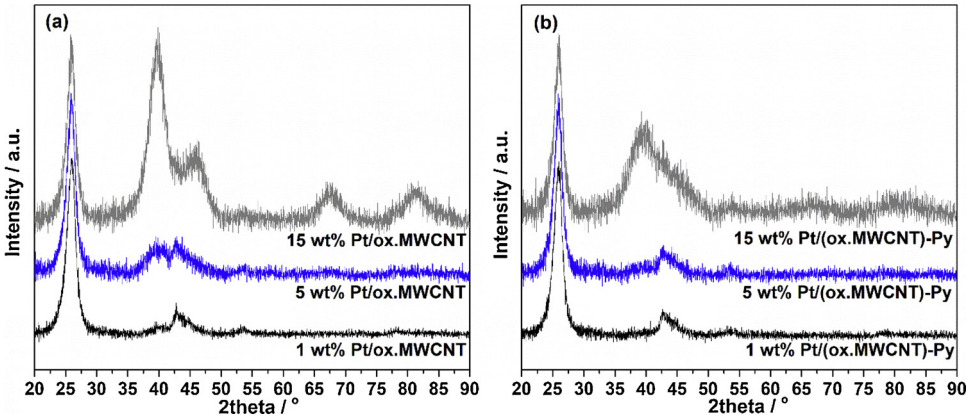

Fig. 1. X-ray diffraction spectra of selected catalysts (a) Pt/ox.MWCNT and (b) Pt/(ox.MWCNT)-Py.

potential deposition (H_{upd}) region. (ii) Evaluation of the oxygen reduction reaction (ORR) activity by cycling in O_2-saturated 0.1 M $HClO_4$ solution at different rotating speeds up to 2500 rpm with 20 mV/s. The anodic scan was used.

3. Results and discussion

Two substrates were used for the platinum deposition, namely oxidized multi wall carbon nanotubes (ox.MWCNT) and the same after functionalization for the covalent attachment of pyridine groups on the surface of the side walls, (ox.MWCNT)-Py [53]. The subsequent metal deposition took place using an optimized modified polyol synthesis as reported in Ref.53 and the amount of the precursor (hexachloroplatinic acid, H_2PtCl_6) was adjusted to result in Pt loadings between 1–30 wt% in relation to the substrate. Powder XRD patterns were obtained for all samples and some examples are presented in Fig. 1. Pt/ox.MWCNT catalysts with loadings up to 5 wt% did not show distinct platinum peaks. At and above 10 wt%, the samples present the major Pt diffraction peaks at around 39.7∘ (1,1,1), 46.2∘ (2,0,0), 67.4∘ (2,2,0), 81.3∘ (3,1,1) and 86.3∘ (2,2,2) reflecting their face-centered cubic (FCC) crystal structure. On the other hand, for the Pt/(ox.MWCNT)-Py catalysts, the peaks are distinct in the case of 30 wt%, visible but flattened for the 15 wt%, while are almost absent for the catalyst with lower Pt loading. Therefore, for most of the samples, it was not possible to calculate the mean particle diameter or other characteristics of Pt using the XRD patterns due to the very small particle size and amount of Pt.

In order to better investigate the actual size and dispersion of the deposited platinum particles, TEM images were obtained for all samples. Selected examples of the images are shown in Fig. 2 and the estimated corresponding mean particle sizes are included in Table 1. It can be seen that the platinum particles supported on ox.MWCNT exhibit a slight variation in size (2.8–3.4 nm) with increasing Pt loading. As the loading increases, almost only the density of the particles increases. Although the metal is present all over the surface of the support (there are no “empty” nanotubes) and the dense presence of functional surface sites (carboxyl, hydroxyl and carbonyl groups) can potentially assist the fine deposition, the distribution of the particles is not uniform but instead larger agglomerates of the smaller particles are observed especially for the case of the higher loading 15 wt% Pt/ox.MWCNT (Fig. 2g), while the particle size distribution is rather wide. A different situation is observed in the case of the catalysts based on (ox.MWCNT)-Py. As reported in a previous work [53], the attached pyridine moieties assist the fine distribution of Pt. This is done either by improving the distribution of nanotubes in the reaction solution and/or through the interactions with the Pt ions of the precursor. In this respect the pyridine moieties on the nanotubes serve as molecular templates and sites for ion adsorption leading to the formation of nucleation centers for the reduction reaction by EG. As shown in Fig. 2 for the 5 wt% and 15 wt% Pt/(ox.MWCNT)-Py samples, the Pt nanoparticles are marked by minimal aggregation, high and uniform dispersion, narrow size distribution and small mean particle diameter close to 2 nm in all cases (Table 1). What is even more interesting is that for 1 and 2 wt% Pt/(ox.MWCNT)-Py, even high resolution TEM did not reveal the presence of any platinum particles. This can be an indication of atomic dispersion. As mentioned, high or atomic dispersion of supported metals is most commonly addressed on oxide supports like ceria, alumina, etc, while is considered challenging to be reached on carbon supports. This would mean that part of the platinum precursor ions was not reduced to Pt^0 in order to lead to the formation of particles. Instead, it reacted or interacted most probably with surface nitrogen containing pyridine groups forming compounds or complexes that are stable under reductive environment and manage to restrain Pt ions on the surface of the substrate.

In order to confirm the presence and evaluate the amount of platinum on the samples, ICP-OES took place and the results are presented in Table 1. The catalysts supported on the pyridine modified substrate have slightly lower platinum loadings than the corresponding catalysts supported on oxidized nanotubes. Nevertheless, the deposition was realized to a satisfactory degree in all cases, reaching loadings close to the nominal.

XPS analysis was carried out in order to investigate the oxidation state of platinum and the results are shown in Fig. 3 and Table 2. In Fig. 3, selected Pt-4f X-ray photoelectron spectra of the electrocatalysts are shown. On ox.MWCNT the predominant species is metallic platinum. Three doublets (high Pt $4f_{5/2}$ and low Pt $4f_{7/2}$ energy band) were used for the deconvolution of the peaks, which correspond to metallic platinum Pt^0 at 71.5–71.8 eV, Pt^{2+} (PtO) around 73.5 eV and Pt^{4+} (PtO_2) around 75.5 eV. The zero-valent platinum peak is about 0.6 eV higher than the value of bulk Pt. This positive shift may be attributed to the small particle size effect [58–60] and/or an interaction with the support (charge transfer between platinum and carbon) [61,62]. The observed BE values are consistent with several reports in literature [63–65]. As the Pt loading increases, a trend of decreasing Pt oxidation states is revealed. Oxygen chemisorption easily occurs at step and kink sites present on the surface of the Pt. Therefore, the higher surface resulting from the smaller particle size can lead to lower metallic over oxidized Pt ratio. The relatively small increase in Pt^0 percentage follows the increase of the particle size (Table 2).

Quite different is the case of Pt/(ox.MWCNT)-Py samples, Table 2. At low platinum loadings, there is an almost complete absence of metallic platinum and the predominant species is Pt^{2+}, thus contributing to the hypothesis for atomic dispersion. Increase in the loading led to increase in the percentage of the zero-valent platinum, nevertheless always with a strong presence of the Pt^{2+} ($Pt^0/Pt^{2+} \approx 1/1$ for Pt loading $\geq$ 10%) as compared to corresponding ox.MWCNT samples

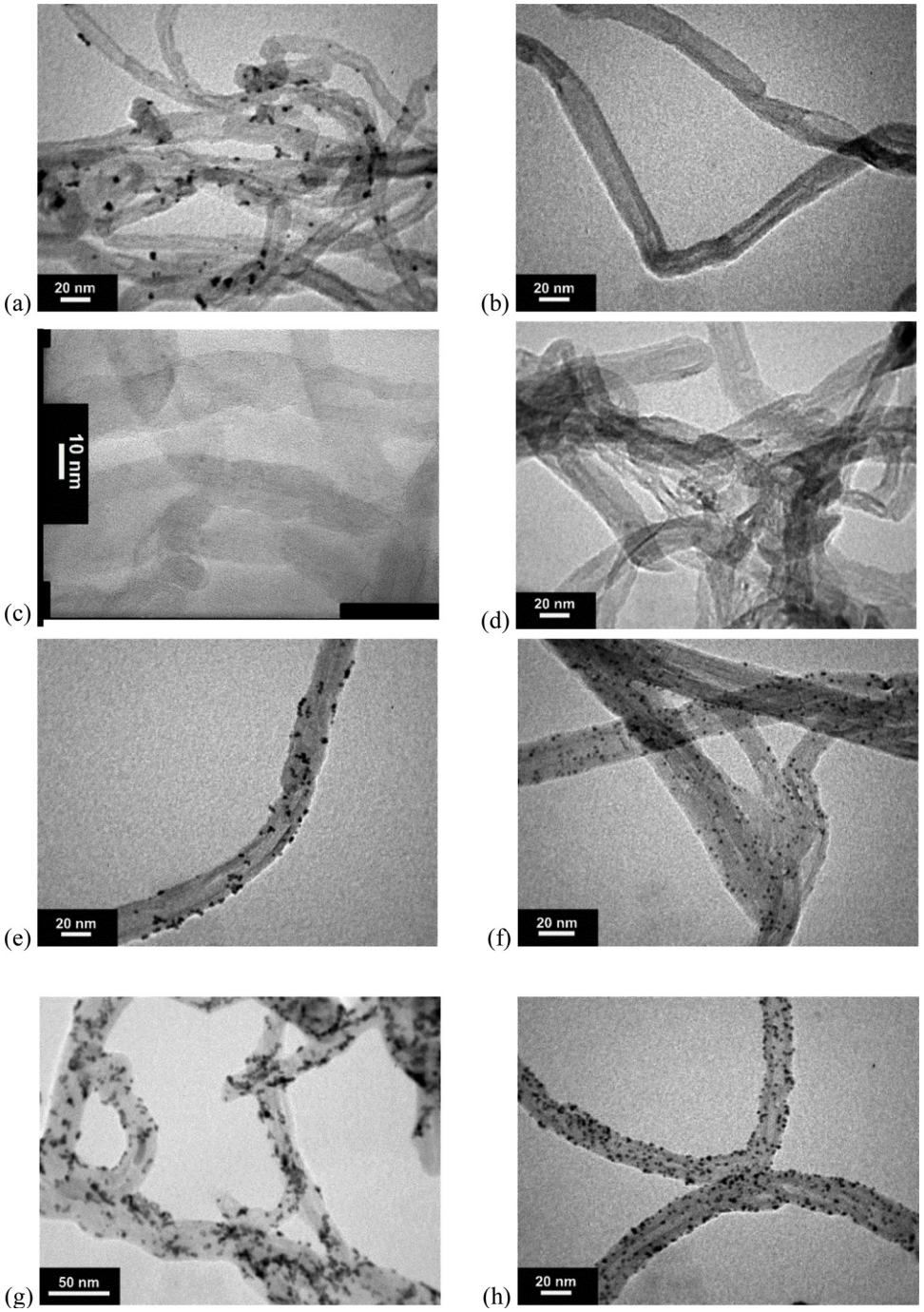

Fig. 2. TEM images of samples (a) 1 wt% Pt/ox.MWCNT, (b) and (c) 1 wt% Pt/(ox.MWCNT)-Py, (d) 2 wt% Pt/(ox.MWCNT)-Py, (e) 5 wt% Pt/ox.MWCNT, (f) 5 wt% Pt/(ox.MWCNT)-Py, (g) 15 wt% Pt/ox.MWCNT and (h) 15 wt% Pt/(ox.MWCNT)-Py. No Pt particles are formed on pyridine modified support (b), (c) and (d), while fine distribution of Pt nanoparticles 1.7–2.9 nm is observed at higher Pt loadings (f) and (h).

Table 1
Platinum mass loading (wt%) from ICP results and mean particle size, d, estimated based on TEM images.

Catalyst	Pt / wt%	d / nm	Catalyst	Pt / wt%	d / nm
1 wt% Pt/ox.MWCNT	0.9	2.8	1 wt% Pt/(ox.MWCNT)-Py	0.8	–
2 wt% Pt/ox.MWCNT	2.0	3.0	2 wt% Pt/(ox.MWCNT)-Py	1.7	–
5 wt% Pt/ox.MWCNT	4.6	2.8	5 wt% Pt/(ox.MWCNT)-Py	4.2	1.7
10 wt% Pt/ox.MWCNT	10	3.0	10 wt% Pt/(ox.MWCNT)-Py	9.1	1.9
15 wt% Pt/ox.MWCNT	15	3.4	15 wt% Pt/(ox.MWCNT)-Py	15	2.3
30 wt% Pt/ox.MWCNT	28	3.4	30 wt% Pt/(ox.MWCNT)-Py	30	2.9

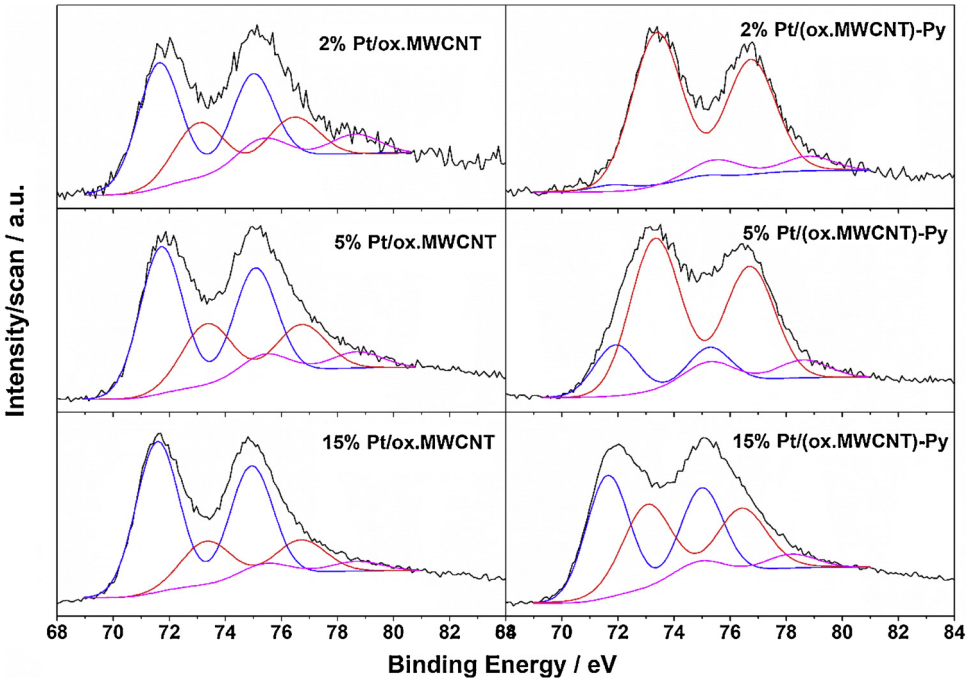

Fig. 3. Selected XPS deconvoluted spectra of the Pt 4f region comparing catalysts with two different substrates, (ox.MWCNT and (ox.MWCNT)-Py) and different Pt loads (2–15 wt%). Pt appears highly oxidized on the pyridine modified substrate, (ox.MWCNT)-Py.

Table 2
Deconvolution of Pt 4f XPS data into single components for all samples. For each chemical signature, BE (eV) and amount (at %) are given. N/Pt, Pt/Cl and C/Pt atomic ratios are also shown.

Nr	Sample name	Oxidation states			N/Pt	Pt/Cl	C/Pt
		State	BE (eV)	Amount (%)			
1	1 wt% Pt/ox.MWCNT	Pt^0	71.8	47.6	–	–	738
		Pt^{2+}	73.7	28.6			
		Pt^{4+}	75.8	23.8			
2	2 wt% Pt/ox.MWCNT	Pt^0	71.6	57.7	–	–	628
		Pt^{2+}	73.1	28.5			
		Pt^{4+}	75.3	13.8			
3	5 wt% Pt/ox.MWCNT	Pt^0	71.7	60.0	–	–	228
		Pt^{2+}	73.3	29.6			
		Pt^{4+}	75.3	10.4			
4	10 wt% Pt/ox.MWCNT	Pt^0	71.5	70.2	–	–	183
		Pt^{2+}	73.3	21.9			
		Pt^{4+}	75.5	7.9			
5	15 wt% Pt/ox.MWCNT	Pt^0	71.6	69.4	–	–	116
		Pt^{2+}	73.3	23.6			
		Pt^{4+}	75.3	7.0			
6	1 wt% Pt/ (ox.MWCNT)-Py	Pt^0	71.7	6.6	33	1.1	609
		Pt^{2+}	73.5	75.9			
		Pt^{4+}	75.5	17.5			
7	2 wt% Pt/ (ox.MWCNT)-Py	Pt^0	71.8	3.6	12	1.06	356
		Pt^{2+}	73.4	85.7			
		Pt^{4+}	75.5	10.7			
8	5 wt% Pt/ (ox.MWCNT)-Py	Pt^0	71.9	19.8	4.8	2.2	113
		Pt^{2+}	73.3	69.4			
		Pt^{4+}	75.3	10.8			
9	10 wt% Pt/ (ox.MWCNT)-Py	Pt^0	71.7	44.4	2.2	3.2	60
		Pt^{2+}	73.2	42.8			
		Pt^{4+}	75.2	12.8			
10	15 wt% Pt/ (ox.MWCNT)-Py	Pt^0	71.6	49.4	1.6	5.0	52
		Pt^{2+}	73.1	41.8			
		Pt^{4+}	74.8	8.8			
11	30 wt% Pt/ (ox.MWCNT)-Py	Pt^0	71.6	49.8	1.2	5.4	47
		Pt^{2+}	73.0	37.2			
		Pt^{4+}	75.0	13.0			

without pyridines. N/Pt and C/Pt ratios decrease with Pt loading as expected. It should be also noted that the high and improved dispersion of nanoparticles in the presence of pyridine is also apparent by considering the surface C/Pt ratio, which is sensibly lower than that of the corresponding samples on oxidized, non-functionalized nanotubes.

The N 1s peaks of samples based on (ox.MWCNT)-Py, including the pure substrate before the platinum deposition, are shown in Fig. 4 (left). The spectra are deconvoluted into two single chemically shifted components. The main feature is the peak at 399 eV, assigned to the pyridinic nitrogen [53,66]. As also reported in Ref. [67] during the functionalization reaction of nanotubes, nitrogen species other than pyridine are also unavoidably created, as evidenced by the peak around 401 eV, generally ascribed to more positively charged nitrogen species. Although the signal of N 1s decreases upon platinum deposition, it is still apparent that the ratio of the peak surface areas at 399 and 401 eV is decreased, concomitant to the enhanced presence of positively charged species [68]. Direct formation of Pt−N bonds between the surface Pt atoms of the nanoparticles and N is unlikely to be formed, since this would shift the N 1s peak to lower binding energies so as to correlate with the increase in the Pt 4f binding energy. Nevertheless, it is rather probable that some interactions take place between Pt and N and the obtained surface chemistry characteristics may delocalize the electron density of Pt. However, the latter would not be easily detectable by the XPS measurements.

According to Yoshida et al. an acidic electrophilic support can decrease the electron density of the 5d band in platinum 69. The acidity/alkalinity of the support seems to influence the formation of platinum oxides. Labou and Neophytides reported a significant effect on the reactivity of oxygen for the catalytic oxidation of H_2 on a PtRu/C catalyst, when it was interfaced with acidic or alkaline solutions [19]. If the support is acidic, the voltage of the electrode is more positive, implying increase of Pt work function thus, resulting in limited availability of the 5d band electrons to form Pt oxides. In this respect, the basic pyridine groups could increase the platinum electron density by shifting the Fermi level thus, causing a decrease in the work function of the Pt surface. This would increase the tendency of platinum to react with oxygen. Along with the smaller particle size obtained that is reported to lead to stronger binding of OH_{ads} [70], this could justify the intense

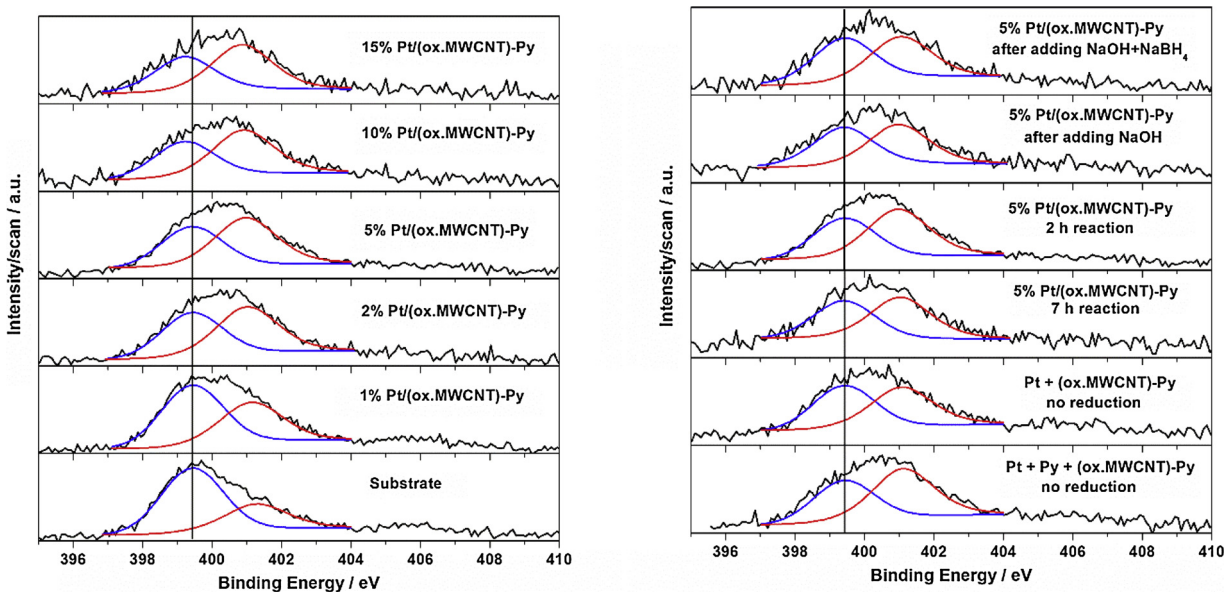

Fig. 4. XPS deconvoluted spectra of the N 1s region of Pt/(ox.MWCNT)-Py catalysts with different Pt loadings (1–15 wt%) (left column). The N 1s peak at 401 eV increases upon Pt deposition indicating chemical interactions with deposited Pt. Right column: 5 wt% Pt/(ox.MWCNT)-Py synthesized in different ways and two samples resulted by mixing platinum precursor with pyridine functionalized nanotubes with no reduction reaction taking place (see samples of Table 3).

Table 3
Deconvolution of Pt 4f XPS data into single components for different Pt/(ox.MWCNT)-Py and unsupported samples, synthesized or treated under different conditions. For each chemical signature, BE (eV) and amount (at%) are given. N/Pt, Pt/Cl and C/Pt ratios are also shown.

Nr	Sample	Oxidation states			N/Pt	Pt/Cl	C/Pt
		State	BE (eV)	Amount (%)			
1	5 wt% Pt/(ox.MWCNT)-Py. 7 h in acidic pH	Pt^0	71.8	24.6	4.5	2.9	158
		Pt^{2+}	73.2	59.6			
		Pt^{4+}	75.1	15.9			
2	5 wt% Pt/(ox.MWCNT)-Py. 2 h in acidic pH + 2 h with $NaBH_4$/NaOH	Pt^0	71.7	29.7	5.2	2.2	162
		Pt^{2+}	73.2	58.6			
		Pt^{4+}	75.1	11.7			
3	2 wt% Pt/(ox.MWCNT)-Py. 2 h in acidic pH + 2 h with $NaBH_4$/NaOH	Pt^0	71.7	6.5	8.7	1.0	255
		Pt^{2+}	73.4	66.1			
		Pt^{4+}	75.7	27.4			
4	5 wt% Pt/(ox.MWCNT)-Py. 2 h in acidic pH + 2 h in basic pH	Pt^0	71.8	24.5	4.9	2.6	143
		Pt^{2+}	73.1	61.5			
		Pt^{4+}	75.0	14.0			
5	Unsupported Pt. Presence of Py in reaction solution	Pt^0	71.5	71.7	–	–	–
		Pt^{2+}	73.4	20.5			
		Pt^{4+}	75.5	7.8			
6	Pt + (ox.MWCNT)-Py. No reduction conditions	Pt^0	–	–	16	0.46	523
		Pt^{2+}	73.2	86.2			
		Pt^{4+}	75.0	13.8			
7	Pt + Py + (ox.MWCNT)-Py. No reduction conditions	Pt^0	–	–	10	0.44	334
		Pt^{2+}	72.9	80.9			
		Pt^{4+}	75.0	19.1			

presence of Pt(II) in the Pt/(ox.MWCNT)-Py samples.

The alarming fact is the appearance of chlorides in the samples based on the pyridine functionalized substrate. Although the amount is relatively small and decreases with the amount of Pt^0, still their presence could indicate an incomplete hexachloroplatinic acid anions' reduction. Willing to eliminate the possibility that the local pH, as defined by the pyridines, retards the reduction reaction of the hexachloroplatinic anions that remain despite the extensive washing of the samples, one sample, namely 5 wt% Pt/(ox.MWCNT)-Py, was chosen and prepared in different ways. The latter included increase of the reaction time from 2 (Table 2) to 7 h or addition of the strong reducing agent $NaBH_4$ in NaOH after the 2 h of initial reaction in acidic environment. For reference, changing the pH from acidic to basic after the reaction completion (2 h in acidic EG solution) also took place. Table 3 shows estimates from XPS results of the aforementioned samples, and as is evident, the variation with respect to both the oxidative state of platinum and the amount of chlorides lies within the experimental error limits.

In this respect, the formation of anionic Pt-oxo-chloro-complexes of Pt(II) existing as counter ions to the pyridinic nitrogen of the carbon support 71 or isolated reduced Pt atoms interacting with the nitrogen containing groups is strongly suggested. The complexes/compounds/interactions are stable under reductive acidic or basic environment, but their exact nature is still difficult to be defined. The N 1s XPS spectra, Fig. 4 (right), are not very informative, because the features of the peaks in all the aforementioned cases are similar. The stability of these Pt(II) complexes were tested under prolonged treatment with NaOH and strongly reducing conditions with $NaBH_4$. The complexes were shown to be stable retaining both the protonation of the pyridinic nitrogen and the chlorides. These complexes appear to be stable at any Pt loading as this is shown for the cases of 2 wt% and 5 wt% samples (Table 3 **samples 2 and 3).** The results depicted in Table 3 show that in the case of the 5 wt% samples Pt nanoparticles are formed and deposited over the Pt(II) complexes, which may act as the substrate. In any case, the existence of chlorides in all pyridine modified samples as the Pt loading increases, Table 2, denotes that these atomically dispersed Pt(II) species co-exist along with small clusters of the metallic Pt.

In an attempt to clarify the nature of the formed Pt(II) compounds, synthesis of unsupported platinum nanoparticles in EG took place. The reaction conditions were kept the same, but instead of dispersing the (ox.MWCNT)-Py support, an amount of liquid pyridine was dissolved in the reaction solution. More specifically, Pt/Py weight ratio initially in the solution was around 3 (atomic ratio ˜ 1.2). Upon reduction, solid nanoparticles were obtained that were further characterized by means of XPS. The Pt 4f spectrum is shown in Fig. 5 and the deconvolution data are depicted in Table 3, **sample 5**. The peak of Pt reveals that metallic platinum dominates. The main peak is at BE = 71.5 eV, slightly shifted to lower values (by 0.2 - 0.3 eV) due to the absence of the support. Nevertheless, the solid contained no notable surface nitrogen. With this synthetic route, either no complexes were formed or the

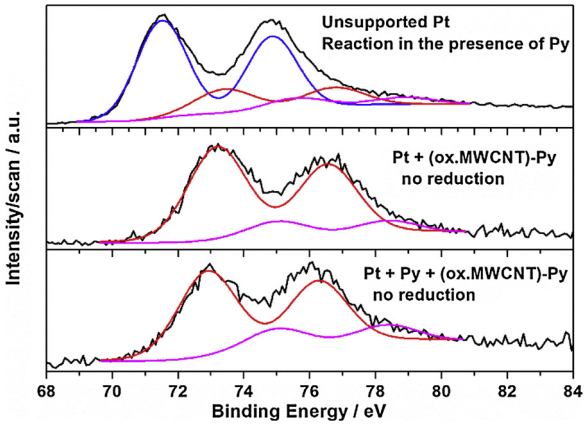

Fig. 5. XPS deconvoluted Pt 4f spectra of unsupported Pt nanoparticles synthesized in the presence of pyridine moieties and two samples resulted by mixing platinum precursor with pyridine functionalized nanotubes with no reduction reaction taking place (with and without additional pyridine in the solution).

produced complexes were water soluble (therefore washed away) or not stable under the reductive environment.

Next step was to simply disperse oxidized or pyridine functionalized nanotubes in an aqueous solution of the platinum precursor (H_2PtCl_6) for the time corresponding to the total reaction time of the actual synthesis of Pt supported catalysts **(**Table 3**, sample 6).** No reductive agent was added, in order to detect the formation of any compounds or strong interactions. "Deposition" of the precursor ions could be expected to some extent, as is the procedure followed in the deposition-reduction synthetic route. Pt ions adsorb onto the surface via coordination or ion-exchange reactions, and serve as the nucleation sites that are eventually reduced to nanoparticles. The XPS analysis of the sample, where the precursor salt was mixed with ox.MWCNT under no reductive conditions, did not present any Pt peak, meaning that no platinum based ions remained to interact with the substrate and all the precursor salt was washed away from the nanotubes. The oxidized nanotubes used in this work are not an effective adsorbent of platinum (IV) chloride ions. Changing the temperature, the solvent or mixing rate could differentiate this result, but it is considered out of the scope of this work.

On the contrary, when (ox.MWCNT)-Py were used, some platinum amount remained attached to the nanotubes. Two experiments took place: (a) only Pt salt and (ox.MWCNT)-Py were present in the solution and (b) the same as in (a) with the addition of pyridine monomers (Table 3 **sample 7**, see experimental section). In both cases, most of the precursor salt amount (initially aiming for a Pt load of 30 wt%) was removed during washing. According to the surface atom ratios (N/Pt and Pt/C) in Table 3 and compared to those in Table 2, the Pt loading reached close to 1 wt% after stirring the precursor with the nanotubes and 2 wt% in the presence of additional pyridine in the solution. The content of chloride atoms is increased by a factor of 2, compared to the 1 and 2 wt% Pt supported catalysts on the same substrate **(**Table 2 **samples 6 and 7).** Looking at the Pt XPS peaks, Fig. 5 and Table 3, Pt^0 is absent as was expected. Although it seemed reasonable to detect only Pt(IV) contained in the hexachloroplatinic acid almost all platinum is in the form of Pt(II).

In parallel, the nitrogen spectra acquired similar features as the low loading Pt supported catalysts of Table 2. The spectra were not dependent on the duration of the XPS measurement, thus partial reduction of the platinum ions caused by the radiation is excluded [72,73]. H.E. van Dam et al observed that activated carbon, upon impregnation, reduced a certain amount of the Pt(IV) forming a Pt(II) complex, which was strongly chemisorbed at the walls of the carrier's mesopores 74. The surface treatment of the support and the chemistry of the impregnation process define the adsorption. Choi et al also reported the spontaneous reduction of metal ions to metal particles on the sidewalls of single walled carbon nanotubes and rationalized it through an electron transfer from the nanotube (oxidation) to the metal ions causing the latter's reduction, as a result of the higher Fermi level of nanotubes compared to the reduction potential of the Pt ions 75. The proposed mechanism requires several steps starting with the diffusion of initial Pt(IV) ions of the precursor to the surface and their adsorption therein, followed by first reduction step to Pt(II) in the form of $(PtCl_4)^{2-}$76The latter is then coordinatively bound to the carrier on a ligand site (either a π-complex structure or an oxygen surface group). In the present case the introduced pyridine based groups are surface basic sites associated with π-electron rich regions and therefore could act as Lewis type bases 77, become protonated (as supported also from XPS spectra in Fig. 4 where the N peak at the higher binding energy increases with increasing Pt loading) and stably anchor $(PtCl_4)^{2-}$ by replacing one of its original Cl^- ligands [11,78]. In the case of the samples and conditions followed in this work, (i) the atomic ratio of Pt(II)/Cl, (ii) the absence of metallic platinum and (iii) the presence of such complexes only in the pyridine functionalized nanotubes and their stability under intense reductive and alkaline conditions (Table 3) do not exclude a similar mechanism at the first steps at least, but certainly do not support this exact scheme.

Nevertheless, the Pt(II) species formed on the (ox.MWCNT)-Py support **(**Table 3**, samples 6 and 7)** without the presence of a reducing agent (EG) are not stable after their exposure to basic solution in contrast to the Pt(II) species formed during the reduction of Pt(IV) in the presence of EG (Table 3**, sample 3**). Thus it can be inferred that the chemical structure of the Pt(II)-oxo-complexes formed during the reduction process (Fig. 3) differs from the chemical structure of the Pt(II) compound that is formed by the chemical interaction of the hexachloroplatinic acid with the pyridine moieties on the support (Fig. 5). Their final form is created and stabilized during the reduction reaction only in acidic environment.

3.1. Electrochemical behavior towards ORR

The electrochemical performance and stability of the electrocatalysts strongly depend on the physicochemical characteristics of the materials, such as their surface area, the crystalline structure, size and shape of the particles and the interactions with the support. The electrochemical characterization took place by means of Rotating Disc Electrode method in 0.1 M $HClO_4$ at room temperature. These measurements are very sensitive to a number of parameters like impurities, electrolyte used, catalytic layer thickness, catalyst type and properties, Pt loading on the catalyst and the presence of ionomer (Nafion) [79,80]. In this work, the catalyst substrate, the Pt loading and the Pt chemical state differ between the samples, rendering the selection of one set of optimum parameters for the electrode preparation very difficult. One simple example is the difference in the hydrophilicity of the substrates used in this work, as proven in a previous work Ref. 56. According to this study the (ox.MWCNT)-Py support is hydrophilic thus expecting to affect the structure of the electrochemical interface.

In this respect, despite keeping constant the measurement conditions (electrolyte, temperature etc), the first aim was to set the rest of the parameters in order to allow a safe comparison. Although it is well established in literature that a calculated Nafion cap thickness < 0.1 - 0.2 μm has no measurable effect on the O_2 limiting current [81,82], it does not preclude any ionomer impact on ORR kinetics. In this respect, and given the many different loadings and features of the synthesized catalysts, the Nafion-free electrode was adopted for this first screening of the electrocatalytic performance 79. To further decrease the variants, in this work the catalytic layer thickness, as it is defined by the carbon nanotubes' amount on the disk, was kept constant in all samples. Following the thin-film RDE method [80–83], in order to optimize the amount of the catalyst on the electrode, we performed tests with

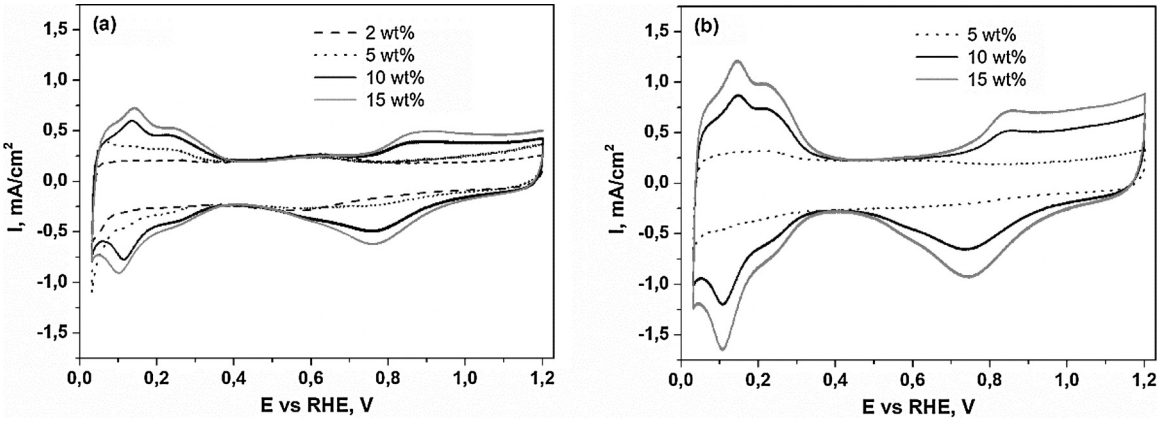

Fig. 6. Cyclic voltammograms in an Ar-saturated 0.1 M $HClO_4$ solution at room temperature with a sweep rate of 100 mV/s for different wt% Pt catalysts supported on (a) ox.MWCNT and (b) (ox.MWCNT)-Py. Carbon nanotube loading is 47 μg/cm^2.

different catalyst amounts on the disk tip. This calibration was done for 30 wt% catalysts and was further confirmed using lower loadings. The results showed that a loading of 47 μg of MWCNTs per cm^2 can provide reliable and reproducible electrokinetic data.

3.2. Electrochemically active vs catalytic surface area

After activation, cyclic voltammograms were recorded in Ar saturated electrolyte solution for each of the prepared catalysts in order to evaluate the electrochemically active surface area, ECSA. Examples of the obtained voltammograms at a scan rate of 100 mV/s are depicted in Fig. 6. ECSA was calculated from the H_{upd} region ($E < 0.4$ V) of the cyclic voltammograms by integration of the peaks of the hydrogen adsorption and desorption areas, with the double layer charging current as a baseline (charge uptake of polycrystalline Pt: 210 μC/cm^2). The results are summarized for the different catalysts in Table 4 expressed as m^2 per g of platinum. For the catalysts with very low loadings and particle size, the ECSA could not be obtained from the hydrogen adsorption/desorption charge due to the low charge and the uncertainty of the background current subtraction. Interestingly the 1 and 2 wt% Pt on (ox.MWCNT)-Py do not show any electrochemical activity as no H_2 UPD/oxidation or O_2 reduction peaks are detected. In the same Table, the catalytic surface area (CSA_{TEM}) as measured by means of TEM histograms is shown too. It must be noted that though the particle size of Pt on the (ox.MWCNT)-Py is smaller than on the non-modified support (Table 1) the CSAs per gram Pt of both catalysts are very close. This is due to the fact that around 2 wt% of Pt is atomically dispersed in the form of inactive complexes on all pyridine modified supports and thus is not visible in the TEM images. As an example, for the 5 wt% Pt/(ox.MWCNT)-Py sample and according to Table 1, the CSA would be 165 m^2 expressed per Pt mass in the form of nanoparticles only. In order to express the CSA with respect to the total Pt mass (as the ECSA value is in the same table), the value is corrected to 86 m^2/g Pt, taking into account both the Pt existing as nanoparticles and the additional mass of 2 wt% inactive Pt in the form of complexes.

The ratio ECSA/CSA is a measure of the electrochemical catalyst utilization, U_{Pt}, of Pt surface atoms participating in the electrochemical reaction. As presented in Table 4, it varies between 65-100% depending on the Pt loading and the type of catalyst support. Shao et al [20] noticed that the electrochemically measured surface areas were found to be significantly less being as low as 60% with respect to the corresponding specific areas calculated from TEM images especially on large Pt particles. They proposed that this can be attributed partly to the occlusion of the Pt particles by the support. In all catalysts of Table 4, the active surface utilization increases with increasing Pt loading. Interestingly the modified (ox.MWCNT)-Py supports show systematically higher utilization (> 20%) than the ox.MWCNT supports, reaching U_{Pt} values within experimental error around 100%. This can be to a certain extent attributed to the hydrophilic character of the (ox.MWCNT)-Py supports [56]. Further especially for the case of ox.MWCNT, the increase of utilization with Pt loading can be attributed to the increase of hydrophilicity of the catalysts. This is because the Pt surface is more hydrophilic, thus compensating the high hydrophobicity of ox.MWCNT. In addition, hydrophobicity of Pt nanoparticles may also depend on the

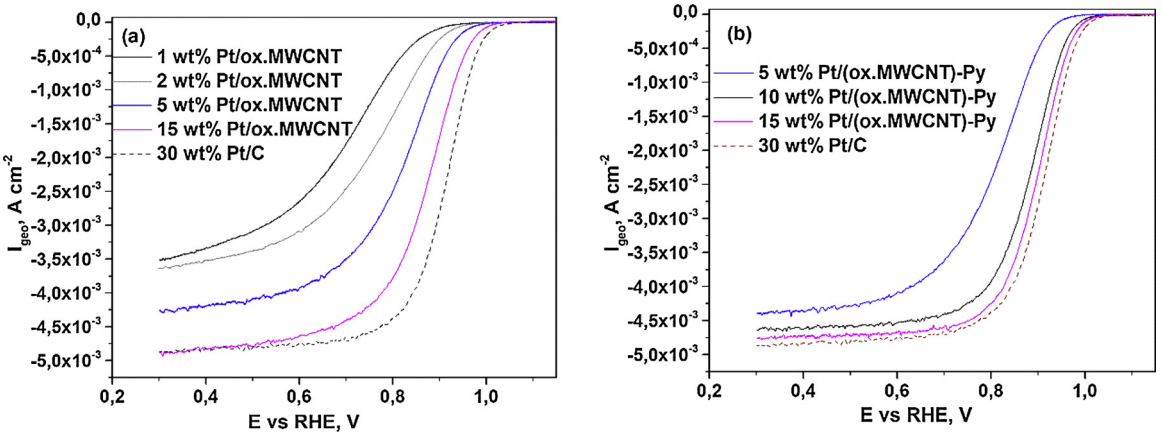

Fig. 7. Polarization curves for oxygen reduction in oxygen saturated 0.1 M $HClO_4$ solution, at 900 rpm and 20 mV/s under oxygen overpressure for (a) catalysts supported on ox.MWCNT and (b) catalysts supported on (ox.MWCNT)-Py. Carbon nanotube loading is constant for all samples at 47 μg/cm^2 so as to achieve the same film thickness for all samples. Pt loading ranges between 0.43 and 20 μg/cm^2.

Table 4
Electrochemical surface area measured by cycling voltammetry, ECSA (m^2 per total grams of Pt), catalytic surface area measured by means of TEM histograms, CSA_{TEM} (m^2 per total grams of Pt), the corresponding electrochemical catalyst utilization, U_{Pt}, and the specific activity, I_{spec}, of each catalyst.

Nr	Sample name	ECSA /m^2/g_{Pt}	CSA_{TEM} * /m^2/g_{Pt}	U_{Pt}/ %	I_{ECSA}/ μA/cm_{Pt}^2	I_{CSA}/ μA/cm_{Pt}^2
1	1wt% Pt/ox.MWCNT	–	100	–	–	218
2	2wt% Pt/ox.MWCNT	–	93	–	–	294
3	5 wt% Pt/ox.MWCNT	65	100	65	519	337
4	10 wt% Pt/ox.MWCNT	62	93	67	585	390
5	15 wt% Pt/ox.MWCNT	60	82	73	505	369
6	30 wt% Pt/ox.MWCNT	70	85	82	394	324
7	5 wt% Pt/(ox.MWCNT)-Py	–	86	–	–	321
8	10 wt% Pt/(ox.MWCNT)-Py	126	115	109	493	540
9	15 wt% Pt/(ox.MWCNT)-Py	108	106	102	476	485
10	30 wt% Pt/(ox.MWCNT)-Py	84	90	93	376	351
11	30 wt% Pt/C	80	93	86	408	351

* CSA_{TEM} in m^2/gPt is calculated according to the equation $CSA_{TEM} = 6000/(21.4*d)$, where d (nm) is the particle diameter from Table 1, given that the density of platinum is 21.4 g/cm^3. For the catalysts supported on pyridine modified support, these values correspond to the total amount of platinum comprising both nanoparticles and the 2 wt% inactive platinum (complexes).

operating potential of the electrochemical interface at which the ECSA is measured or the ORR is carried out. Thus, the wetting of catalysts can vary when moving from the low voltage H_2 region to the high voltage ORR region. In this respect, it must be stressed that the calculated ECSA is possibly underestimated and may not represent the actual surface used in the oxygen reduction reaction especially in the case of ox.MWCNT. In this respect the specific activity is critically discussed below depending on the use of the ECSA or the catalytically active surface area (CSA).

3.3. Oxygen reduction kinetics

Examples of the polarization curves for oxygen reduction in oxygen saturated 0.1 M $HClO_4$ solution, recorded at 900 rpm at a sweep rate of 20 mV/s, are depicted in Fig. 7. In the case of the ox.MWCNT support, all catalysts show activity towards ORR. As expected, the measured current increases with Pt loading, since the mass of Pt is increased. As explained in the experimental section, the carbon amount was kept the same for all samples, to make sure that the catalytic layer thickness was constant and the diffusion resistance is negligible especially within the kinetic region, not affecting the kinetic current in all electrode samples. According to the literature, Pt loading on the glassy carbon ranges between 7–30 μgPt cm^{-2} for catalysts having concentrations of 10–50 wt% Pt on carbon [84]. This could not be followed for the low loading samples of this work, since it would lead to very high amounts of catalyst and thick catalytic layers inducing mass transport limitation issues. Reduced Pt loadings on the support increase the interparticle distance, which, as discussed in literature may influence the observed electrocatalytic activity [85–87]. Among others, it is suspected to lead in a different oxygen reduction reaction mechanism, where a two-electron pathway towards hydrogen peroxide dominates. To elucidate this, normally a rotating ring-disk study is required. Nevertheless, by using the Koutecky-Levich (K-L) equation at different rotating speeds and at 0.3 V, the number of electrons transferred was calculated for the catalysts reported herein and in all cases was found to be very close to 4. Diffusion-limited current is not a function of platinum loading according to the Levich equation. In our materials the limiting current especially at the low Pt loadings is influenced by Pt particle distribution, the degree of the coverage of the forefront layer of the electrode by the Pt particles and the specific surface area of the Pt nanoparticles within the catalytic layer. The theoretical limiting current is directly determined by the diffusion flux of the O_2 molecules through the geometric surface area of the RDE disk and is reached for Pt loadings ≥ 10 wt% for both substrates. In the case of the low loading samples, 1–5 wt%, the specific surface area (0.42-2.1 cm^2/cm_{geo}^2) is less or comparable to the geometric surface of the electrode disk. Thus, it is expected that the limiting current will reach values less than the maximum value. This behavior does not affect the validity of the kinetic current estimation according to the Koutecký-Levich equation especially when the kinetic current is expressed in terms of Pt mass loading on the electrode or in terms of specific surface area of Pt particles.

1 and 2 wt% Pt on (ox.MWCNT)-Py showed no activity towards oxygen reduction, denoting that the existing atomically dispersed Pt^{2+} is indeed completely inactive for the ORR. This reveals that the nanoparticles of platinum at higher loadings is the active ORR catalyst. Choi et al [42] reported the synthesis of a sulphur modified carbon material which can stabilize 5 wt% Pt in the form of atomically dispersed Pt. The results from rotating ring-disk electrode experiments showed that the catalyst has activity towards ORR, but does not follow the conventional 4 electron pathway producing H_2O. Instead selectively catalyzes a 2 electron pathway producing H_2O_2. In the present study, the formed Pt (II)-nitrogen-cloro-oxo complexes are electrochemically inactive. This platinum amount corresponds to about 2 wt% in each sample and to a certain part of the Pt^{2+} observed in the XPS spectra. As is discussed below and shown in Figs. 8 and 9 this amount is subtracted in order to express the mass activity and the specific activity. By increasing the Pt loading on the same substrate, the activity towards ORR is enhanced due to the formation of Pt nanoparticles. Very importantly, despite the low Pt^o percentage as this was determined by the XPS results in Table 2, the catalysts with metal loading ranging between 5–15 wt% depict notably promoted activity. Indicatively, the as prepared Pt/(ox.MWCNT)-Py catalysts with Pt loading 5 and 10 wt% have only 20 and 45 at% of Pt^o (atomic ratio) respectively, with respect to the total Pt amount, while the Pt/ox.MWCNT catalysts with the same loadings possess 60–70 at% Pt^o.

Fig. 8**a** shows the calculated mass (I_{mass}, A/g_{Pt}) activity values, corresponding to the kinetic current at 0.9 V normalized to the total platinum mass deposited as detected by ICP. Moreover, the mass normalized Tafel plots of the estimated kinetic current, I_{kin}, are depicted in Fig. 8**b**. Pt/ox.MWCNT showed decreased mass activity at low Pt loadings, which could be an effect of the inter-particle distance [86]. Note that the particle size, Table 1 and their distribution do not vary considerably. The mass activity stabilizes at around 300–350 A/gPt for Pt loadings ≥ 5 wt% on the ox.MWCNT support. Particle size dependent mass activity has been reported in literature. Shao et al [20] explained that the sharp decrease in ORR activity below 2.2 nm can be attributed to the increased presence of Pt atoms localized at the edges of the cubo-octahedral particle that strongly bind oxygen and the concomitant decrease of the percentage of the Pt atoms on the facet planes that are more reactive for the ORR. As shown in Fig. 8**a** the screening of the electrocatalytic activity of the various electrocatalysts by the use of RDE setup shows a significant increase in the mass activity of (ox.MWCNT)-Py catalysts, which in the case of 10 wt% is by 1.7 times higher than in the case of non-functionalized 10 wt% Pt/ox.MWCNT

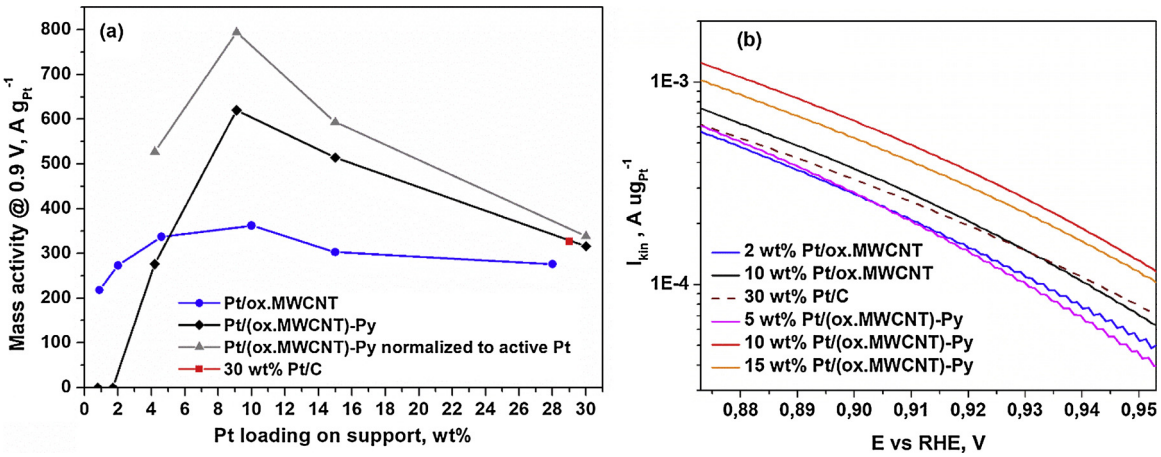

Fig. 8. (a) Mass activity values at 0.9 V and (b) Pt mass normalized Tafel plots towards ORR for different catalysts supported on oxidized or pyridine functionalized nanotubes, as derived using the RDE method in 0.1 M $HClO_4$ solution at room temperature.

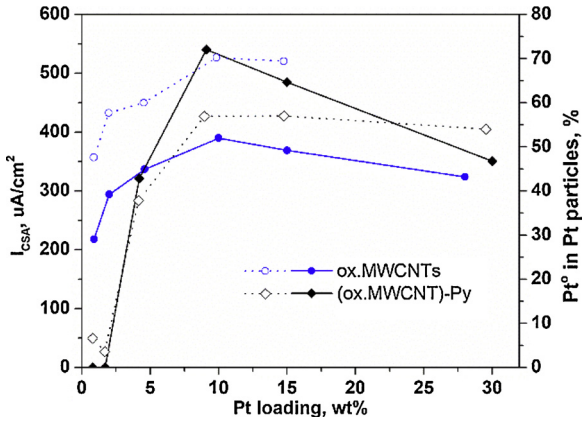

Fig. 9. The effect of Pt loading on active area specific activity, I_{CSA} closed symbols (Table 4), and on metallic Pt^0 content in the Pt nanoparticles (Table 2). Note that for the catalysts supported on pyridine modified support, the metallic content values are normalized by subtracting the 2 wt% inactive platinum in the form of Pt(II) complexes.

and more than twofold increase with respect to the 30 wt% loading on all supports. It is important to mention that the catalysts supported on the pyridine modified substrate include a part of platinum, about 2 wt% in the form of nitrogen-cloro-oxo complexes, which is inactive towards ORR, (see Fig. 8**a** where the 1 and 2 wt% on (oxMWCNT)-Py catalysts are completely inactive for the ORR). In this sense, the mass activity with respect to the active platinum is underestimated, especially in the case of low loading catalysts. A rough idea is presented in Fig. 8**a** (grey symbols), where the mass activity is normalized to the estimated mass of active platinum nanoparticles i.e. by subtracting the mass of the non-active part which, as already mentioned, is around 2 wt%. As becomes apparent, the polar surface groups and the co-existence of Pt(II) complexes with metallic Pt^o induced differentiations in the properties of the latter. This effect fades out as the Pt loading increases, like in the case of 30 wt% Pt/(ox.MWCNT)-Py, which shows similar activity to 30 wt% Pt/ox.MWCNT. Despite the unquestionably superior dispersion and narrow size distribution of platinum on the pyridine modified nanotubes (TEM images), other factors like the size or inter-particle distance could affect the activity, implying a multi-parametric effect of the support on the electrocatalytic activity. It should be stressed that the set of catalysts prepared in this work have different morphological and physicochemical features. The particle size, shape and probably surface morphology, the quality of nanoparticle distribution and the inter-particle distance change significantly with the loading and the type of substrate. In this respect it is very hard to follow a certain trend and understand which effect dominates. Preparing model catalysts to control each characteristic could only separate each effect. The experimental evidence herein, depicted in Fig. 8, shows that Pt nanoparticles are electrocatalytic promoted for the ORR when supported on a modified carbon support, which is covered by atomically dispersed Pt in the form of nitrogen-cloro-oxo complexes. Such a substrate can accommodate the Pt nanoparticles and plausibly induce electronic variations on the surface of platinum nano-crystals (d-band center shift [88,89],) and/or geometric effects.

In Table 4, the specific activity, I_{ECSA}, i.e. the kinetic current normalized with respect to the measured ECSA from the cyclic voltammograms, is depicted for the catalysts with metal loading > 5 wt%. If we consider the ECSA measurements reliable, the catalysts supported on ox.MWCNT show high values, above 500 μA/cm_{Pt}^2, for the loadings 5–15 wt%, while it drops down to about 394 μA/cm_{Pt}^2, close to the conventional 30 wt% Pt/C. The corresponding values for 10 and 15 wt % Pt/(ox.MWCNT)-Py are somewhat lower, almost reaching 500 μA/cm_{Pt}^2. The particle size of ox.MWCNT based platinum nanoparticles (Table 1) is higher than that on pyridine modified substrate. Literature strongly supports size-dependent activity [20,90–92], which could justify the difference between the two supports. Nevertheless, the decrease of I_{ECSA} when going from 15 to 30 wt% loading seems to oppose the reported observations on the interparticle distance and size effect. As already mentioned, the electrochemical determination of the electrochemical surface area, especially in the case of the ox.MWCNT supports, is characterized by certain shortcomings especially at lower loadings thus, leading to the underestimation of the ECSA [20]. A good electrode wettability with aqueous electrolytes, depending on surface potential dependent hydrophilicity is necessary for reliable activity evaluation. In this respect we propose the comparison of specific activity based on CSA instead of ECSA. Fig. 9 shows the surface specific activity I_{CSA}, calculated by normalizing the kinetic current with respect to CSA (Table 4), plotted against Pt loading. I_{CSA} is maximized for both catalytic systems at 10 wt% loading and far more interestingly the enhancement of the electrocatalytic activity observed on the pyridine modified system (ox.MWCNT)-Py is up to 50% higher than the ox.MWCNT. Both systems show a significant increase in the specific activity when moving from the low loading values to the maximum of I_{CSA}, while a rather shallow decrease is observed at higher loadings after the maximum especially for the ox.MWCNT. In addition, at higher Pt loadings both activities decrease and tend to equalize at the highest Pt loading.

Based on the aforementioned spectroscopic evidence by the use of XPS, these variations in I_{CSA} can be correlated to the variation of the amount/percentage of the Pt^{2+} oxide phase, detected by XPS, in the Pt particles (Table 2). Specifically the Pt particles in the pyridine modified

catalysts contain systematically twice as much Pt^{2+} species than the ox.MWCNT samples. This is above and beyond the initial about 2 wt% Pt that participates in the surface Pt(II) complexes. This correlation implies that these Pt oxide species may play a dominant role on the surface chemistry of the Pt^{o} surface atoms. The variation of the oxidation states of Pt within the particle is expected to induce variations of the surface electronic properties (Fermi level, work function) and thus, on the binding strength of oxygen on the Pt surface. It is rather plausible that by modifying the carbon support we can tune the oxidation degree of the Pt particle and control the binding strength and reactivity of adsorbed oxygen species on the Pt surface. However as shown in Fig. 9 especially for the case of (ox.MWCNT)-Py, very high oxidation degree of Pt (as in loadings < 10 wt%) rather inhibits the ORR by preventing the adsorption of O_2.

The above correlation can provide an indicative direction in order to get a deeper insight regarding the metal support interactions for these systems. Nevertheless, certain issues cannot be understood as it is the appearance of maximum activity at the intermediate loadings given the fact that the Pt particle size distribution is not drastically different on the same support and especially at Pt loadings higher than 10 wt%. Although, the inter-particle distance effect has been vaguely mentioned in the literature, the observed variations herein can be rather interpreted by considering that the effect of the support on Pt catalytic properties becomes weaker at increased Pt loading.

4. Conclusions

In conclusion it can be said that the pyridine modified MWCNT supports can be quite promising for the accommodation of low Pt loadings by affecting three decisive factors that define efficient metal support interactions:

- The morphology of the Pt particles. During the initial stages of Pt deposition, Pt is atomically dispersed in the form of Pt(II) nitrogen-cloro-oxo complexes, which form the substrate for the development of finely distributed 1.7–2.9 nm Pt nanoparticles.
- The promotion of the catalytic activity: Both mass and active catalytic surface specific activities are significantly enhanced (> 1.7 times) with respect to the non-modified samples. This can be attributed to the effect of Pt(II) complexes substrate in combination to the induced oxidation degree of the nanoparticles. The latter is defined by its content in Pt oxides.
- It enhances Pt utilization. Pt utilization reaches 100% due to the hydrophilic character of pyridine modified support, which increases the extent and functionality of the electrochemical interface.

Acknowledgements

Mr. George Traskas (Analytical Services Unit (ASU) of CPERI/CERTH) and Dr. Mary Kollia (Lab of Electron Microscopy and Microanalysis, University of Patras) are greatly acknowledged for their help with the ICP-OES and TEM measurements, respectively. This work has been financed by General Secretariat for Research and Technology (GSRT) and Hellenic Foundation for Research and Innovation (HFRI). Part of this work was performed in the framework of the PROENYL project (448305) within the KRIPIS action, funded by Greece and the European Regional Development Fund of the European Union under the O.P. Competitiveness and Entrepreneurship.

References

[1] C. Yang, P. Constamagna, S. Srinivasan, J. Benziger, A.B. Bocarsly, Approaches and technical challenges to high temperature operation of proton exchange membrane fuel cells, J. Power Sources 103 (2001) 1–9, https://doi.org/10.1016/S0378-7753(01)00812-6.

[2] J. Larminie, A. Dicks, Fuel Cell Systems Explained, second ed., John Wiley & Sons Ltd., Chichester, 2003.

[3] J.K. Nørskov, J. Rossmeis, A. Logadottir, L. Lindqvist, J.R. Kitchin, T. Bligaard, H. Jónsson, Origin of the overpotential for oxygen reduction at a fuel-cell cathode, J. Phys. Chem. B 108 (2004) 17886–17892, https://doi.org/10.1021/jp047349j.

[4] V.R. Stamenkovic, B. Fowler, B.S. Mun, G.F. Wang, P.N. Ross, C.A. Lucas, N.M. Markovic, Improved oxygen reduction activity on $Pt_3Ni(111)$ via increased surface site availability, Science 315 (2007) 493–497, https://doi.org/10.1126/science.1135941.

[5] H.A. Gasteiger, S.S. Kocha, B. Sompalli, F.T. Wagner, Activity benchmarks and requirements for Pt, Pt-alloy, and non-Pt oxygen reduction catalysts for PEMFCs, Appl. Catal. B-Environ. 56 (2005) 9–35, https://doi.org/10.1016/j.apcatb.2004.06.021.

[6] D. Notter, K. Kouravelou, T. Karachalios, M.K. Daletou, N.T. Haberland, Life cycle assessment of PEM FC applications: electric mobility and μ-CHP, Energy Environ. Sci. 5 (2015) 1969–1985.

[7] G. Rothenberg, Catalysis: Concepts and Green Applications, 1st ed., Wiley-VCH, 2008.

[8] Y. Cai, R.R. Adzic, Platinum monolayer electrocatalysts for the oxygen reduction reaction: improvements induced by surface and subsurface modifications of cores, Adv. Phys. Chem. 2011 (2011) 530397, , https://doi.org/10.1155/2011/530397.

[9] M. Flytzani-Stephanopoulos, B.C. Gates, Atomically dispersed supported metal catalysts, Annu. Rev. Chem. Biomol. Eng. 3 (2012) 545–574, https://doi.org/10.1146/annurev-chembioeng-062011-080939.

[10] F. Rodriguez-reinoso, The role of carbon materials in heterogeneous catalysis, Carbon 36 (1998) 159–175, https://doi.org/10.1016/S0008-6223(97)00173-5.

[11] X. Yu, S. Ye, Recent advances in activity and durability enhancement of Pt/C catalytic cathode in PEMFC: part I. Physico-chemical and electronic interaction between Pt and carbon support, and activity enhancement of Pt/C catalyst, J. Power Sources 172 (2007) 133–144, https://doi.org/10.1016/j.jpowsour.2007.07.049.

[12] L. Xin, F. Yang, S. Rasouli, Y. Qiu, Z.-F. Li, A. Uzunoglu, C.-J. Sun, Y. Liu, P. Ferreira, W. Li, Y. Ren, L.A. Stanciu, J. Xie, Understanding Pt nanoparticle anchoring on graphene supports through surface functionalization, ACS Catal. 6 (2016) 2642–2653, https://doi.org/10.1021/acscatal.5b02722.

[13] N.M. Markovic, T.G. Schmidt, V. Stamenkovic, P.N. Ross, Oxygen reduction reaction on Pt and Pt bimetallic surfaces: a selective review, Fuel Cells Weinh. (Weinh) 1 (2001) 105–116, https://doi.org/10.1002/1615-6854(200107)1:2<105:AID-FUCE105>3.0.CO;2-9.

[14] N.M. Markovic, H.A. Gasteiger, P.N. Ross Jr., Oxygen reduction on platinum low-index single-crystal surfaces in sulfuric acid solution: rotating Ring-Pt(hkl) disk studies, J. Phys. Chem. 99 (1995) 3411–3415, https://doi.org/10.1021/j100011a001.

[15] F. El Kadiri, R. Faure, R. Durand, Electrochemical reduction of molecular oxygen on platinum single crystals, J. Electroanal. Chem. Lausanne (Lausanne) 301 (1991) 177–188, https://doi.org/10.1016/0022-0728(91)85468-5.

[16] N. Markovic, H. Gasteiger, P.N. Ross, Kinetics of oxygen reduction on Pt(hkl) electrodes: implications for the crystallite size effect with supported Pt electrocatalysts, J. Electrochem. Soc. 144 (1997) 1591–1597, https://doi.org/10.1149/1.1837646.

[17] N.M. Marković, P.N. Ross, Surface science studies of model fuel cell electrocatalysts, Surf. Sci. Rep. 45 (2002) 117–229, https://doi.org/10.1016/S0167-5729(01)00022-X.

[18] Y. Liu, L. Zhang, B.G. Willis, W.E. Mustain, Importance of particle size and distribution in achieving high-activity, high-stability oxygen reduction catalysts, ACS Catal. 5 (2015) 1560–1567, https://doi.org/10.1021/cs501556j.

[19] D. Labou, S.G. Neophytides, Promotional effects on a PtRu/C catalyst-electrode interfaced with aqueous electrolytes: electrochemical metal support interaction (EMSI) and electrochemical promotion of catalysis (EPOC), Top. Catal. 44 (2007) 451–460, https://doi.org/10.1007/s11244-006-0137-z.

[20] M. Shao, A. Peles, K. Shoemaker, Electrocatalysis on platinum nanoparticles: particle size effect on oxygen reduction reaction activity, Nano Lett. 11 (2011) 3714–3719, https://doi.org/10.1021/nl2017459.

[21] T. Imaoka, H. Kitazawa, W.-J. Chun, S. Omura, K. Albrecht, K. Yamamoto, Magic number Pt_{13} and misshapen Pt_{12} clusters: which one is the better catalyst? J. Am. Chem. Soc. 135 (2013) 13089–13095, https://doi.org/10.1021/ja405922m.

[22] Q. Fu, H. Saltsburg, M. Flytzani-Stephanopoulos, Active nonmetallic Au and Pt species on ceria-based water-gas shift catalysts, Science 301 (2003) 935–938, https://doi.org/10.1126/science.1085721.

[23] Y.G. Wang, D.H. Mei, V.A. Glezakou, J. Li, R. Rousseau, Dynamic formation of single-atom catalytic active sites on ceria-supported gold nanoparticles, Nat. Commun. 6 (2015) 6511, https://doi.org/10.1038/ncomms7511.

[24] N. Yi, H. Saltsburg, M. Flytzani-Stephanopoulos, Hydrogen production by dehydrogenation of formic acid on atomically dispersed gold on ceria, ChemSusChem 6 (2013) 816–819, https://doi.org/10.1002/cssc.201200957.

[25] J. Lin, A. Wang, B. Qiao, X. Liu, X. Yang, X. Wang, J. Liang, J. Li, J. Liu, T. Zhang, Remarkable performance of $Ir_1/FeO(x)$ single-atom catalyst in water gas shift reaction, J. Am. Chem. Soc. 135 (2013) 15314–15317, https://doi.org/10.1021/ja408574m.

[26] H. Wei, X. Liu, A. Wang, L. Zhang, B. Qiao, X. Yang, Y. Huang, S. Miao, J. Liu, Y. Zhang, FeOx-supported platinum single-atom and pseudo-single-atom catalysts for chemoselective hydrogenation of functionalized nitroarenes, Nat. Commun. 5 (2014) 5634, https://doi.org/10.1038/ncomms6634.

[27] Y. Shi, C. Zhao, H. Wei, J. Guo, S. Liang, A. Wang, T. Zhang, J. Liu, T. Ma, Single-atom catalysis in mesoporous photovoltaics: the principle of utility maximization, Adv. Mater. 26 (2014) 8147–8153, https://doi.org/10.1002/adma.201402978.

[28] J. Lin, B. Qiao, N. Li, L. Li, X. Sun, J. Liu, X. Wang, T. Zhang, Little do more: a highly effective $Pt_1/FeOx$ single-atom catalyst for the reduction of NO by H_2, Chem. Commun. (Camb.) 51 (2015) 7911–7914, https://doi.org/10.1039/C5CC00714C.

[29] J.C. Matsubu, V.N. Yang, P. Christopher, Isolated metal active site concentration and stability control catalytic CO_2 reduction selectivity, J. Am. Chem. Soc. 137 (2015) 3076–3084, https://doi.org/10.1021/ja5128133.

[30] E.J. Peterson, A.T. DeLaRiva, S. Lin, R.S. Johnson, H. Guo, J.T. Miller, J.H. Kwak, C.H.F. Peden, B. Kiefer, L.F. Allard, F.H. Ribeiro, A.K. Datye, Low-temperature carbon monoxide oxidation catalysed by regenerable atomically dispersed palladium on alumina, Nat. Commun. 5 (2014) 4885, https://doi.org/10.1038/ncomms5885.

[31] C.K. Narula, L.F. Allard, G.M. Stocks, M. Moses-DeBusk, Remarkable NO oxidation on single supported platinum atoms, Sci. Rep. 4 (2014) 7238, https://doi.org/10.1038/srep07238.

[32] Z.Y. Li, Z. Yuan, X.N. Li, Y.X. Zhao, S.G. He, CO oxidation catalyzed by single gold atoms supported on aluminum oxide clusters, J. Am. Chem. Soc. 136 (2014), https://doi.org/10.1021/ja508547z 14307-14013.

[33] L.C. Grabow, A.A. Gokhale, S.T. Evans, J.A. Dumesic, M. Mavrikakis, Mechanism of the water gas shift reaction on Pt: first principles, experiments, and microkinetic modeling, J. Phys. Chem. C 112 (2008) 4608–4617, https://doi.org/10.1021/jp7099702.

[34] R. Si, J. Raitano, N. Yi, L. Zhang, S.-W. Chan, M. Flytzani-Stephanopoulos, Structure sensitivity of the low-temperature water-gas shift reaction on Cu–CeO_2 catalysts, Catal. Today 180 (2012) 68–80, https://doi.org/10.1016/j.cattod.2011.09.008.

[35] M. Flytzani-Stephanopoulos, Gold atoms stabilized on various supports catalyze the water-gas shift reaction, Acc. Chem. Res. 47 (2014) 783–792, https://doi.org/10.1021/ar4001845.

[36] Q. Fu, W.-X. Li, Y. Yao, H. Liu, H.-Y. Su, D. Ma, X.-K. Gu, L. Chen, Z. Wang, H. Zhang, B. Wang, X. Bao, Interface-confined ferrous centers for catalytic oxidation, Science 328 (2010) 1141–1144, https://doi.org/10.1126/science.1188267.

[37] K. Sasaki, F. Takasaki, Z. Noda, S. Hayashi, Y. Shiratori, K. Ito, Alternative electrocatalyst support materials for polymer electrolyte fuel cells, ECS Trans. 33 (2010) 473–482, https://doi.org/10.1149/1.3484545.

[38] S. Sun, G. Zhang, N. Gauquelin, N. Chen, J. Zhou, S. Yang, W. Chen, X. Meng, D. Geng, M.N. Banis, R. Li, S. Ye, S. Knights, G.A. Botton, T.-K. Sham, X. Sun, Single-atom catalysis using Pt/Graphene achieved through atomic layer deposition, Sci. Rep. 3 (2013) 1775, https://doi.org/10.1038/srep01775.

[39] H. Yan, H. Cheng, H. Yi, Y. Lin, T. Yao, C. Wang, J. Li, S. Wei, J. Lu, Single-atom Pd_1/Graphene catalyst achieved by atomic layer deposition: remarkable performance in selective hydrogenation of 1,3-butadiene, J. Am. Chem. Soc. 137 (2015) 10484–10487, https://doi.org/10.1021/jacs.5b06485.

[40] S. Proch, M. Wirth, H.S. White, S.L. Anderson, Strong effects of cluster size and air exposure on oxygen reduction and carbon oxidation electrocatalysis by size-selected Pt(n) ($n \leq 11$) on glassy carbon electrodes, J. Am. Chem. Soc. 135 (2013) 3073–3086, https://doi.org/10.1021/ja309868z.

[41] X. Zhang, J. Guo, P. Guan, C. Liu, H. Huang, F. Xue, X. Dong, S.J. Pennycook, M.F. Chisholm, Catalytically active single-atom niobium in graphitic layers, Nat. Commun. 4 (2013) 1924, https://doi.org/10.1038/ncomms2929.

[42] C.H. Choi, M. Kim, H.C. Kwon, S.J. Cho, S. Yun, H.-T. Kim, K.J.J. Mayrhofer, H. Kim, M. Choi, Tuning selectivity of electrochemical reactions by atomically dispersed platinum catalyst, Nat. Comm. 7 (2016) 10922, https://doi.org/10.1038/ncomms10922.

[43] S. Iijima, Helical microtubules of graphitic carbon, Nature 354 (1991) 56–58, https://doi.org/10.1038/354056a0.

[44] S. Iijima, T. Ichihashi, Single-shell carbon nanotubes of 1-nm diameter, Nature 363 (1993) 603–605, https://doi.org/10.1038/363603a0.

[45] Y. Xing, Synthesis and electrochemical characterization of uniformly-dispersed high loading Pt nanoparticles on sonochemically-treated carbon nanotubes, J. Phys. Chem. B 108 (2004) 19255–19259, https://doi.org/10.1021/jp046697i.

[46] S. Sun, D. Yang, G. Zhang, E. Sacher, J.-P. Dodelet, Synthesis and characterization of platinum nanowire–Carbon nanotube heterostructures, Chem. Mater. 19 (2007) 6376–6378, https://doi.org/10.1021/cm7022949.

[47] R. Kannan, B.A. Kakade, V.K. Pillai, Polymer electrolyte fuel cells using nafion-based composite membranes with functionalized carbon nanotubes, Angew. Chem. Int. Ed. 47 (2008) 2653–2656, https://doi.org/10.1002/anie.200704343.

[48] M.M. Shaijumon, S. Ramaprabhu, N. Rajalakshmi, Platinum/multiwalled carbon nanotubes-platinum/carbon composites as electrocatalysts for oxygen reduction reaction in proton exchange membrane fuel cell, Appl. Phys. Lett. 88 (2006) 253105, , https://doi.org/10.1063/1.2214139.

[49] W. Li, C. Liang, J. Qiu, W. Zhou, H. Han, Z. Wei, G. Sun, Q. Xin, Carbon nanotubes as support for cathode catalyst of a direct methanol fuel cell, Carbon 40 (2002) 791–794, https://doi.org/10.1016/S0008-6223(02)00039-8.

[50] J.M. Tang, K. Jensen, M. Waje, W. Li, P. Larsen, K. Pauley, Z. Chen, P. Ramesh, M.E. Itkis, Y. Yan, R.C. Haddon, High performance hydrogen fuel cells with ultralow Pt loading carbon nanotube thin film catalysts, J. Phys. Chem. C 111 (2007) 17901–17904, https://doi.org/10.1021/jp071469k.

[51] P. Serp, M. Corrias, P. Kalck, Carbon nanotubes and nanofibers in catalysis, Appl. Catal. A Gen. 253 (2003) 337–358, https://doi.org/10.1016/S0926-860X(03)00549-0.

[52] R.V. Hull, L. Li, Y. Xing, C.C. Chusuei, Pt nanoparticle binding on functionalized multiwalled carbon nanotubes, Chem. Mater. 18 (2006) 1780–1788, https://doi.org/10.1021/cm0518978.

[53] A. Orfanidi, M.K. Daletou, S.G. Neophytides, Preparation and characterization of Pt on modified multi-wall carbon nanotubes to be used as electrocatalysts for high temperature fuel cell applications, Appl. Catal. B: Environ. 106 (2011) 379–389, https://doi.org/10.1016/j.apcatb.2011.05.043.

[54] J.K. Kallitsis, A.K. Andreopoulou, M. Daletou, S. Neophytides, High temperature polymer electrolyte fuel cells-approaches, Status and perspectives, Ch. 5, in: J.O. Jensen, D. Aili, H.A. Hjuler, Q. Li (Eds.), Pyridine Containing Aromatic Polyether Membranes, 2016, pp. 91–126.

[55] M.K. Daletou, M. Geormezi, E. Vogli, G.A. Voyiatzis, S.G. Neophytides, The interaction of H_3PO_4 and steam with PBI and TPS polymeric membranes. A TGA and Raman study, J. Mater. Chem. A Mater. Energy Sustain. 2 (2014) 1117–1127, https://doi.org/10.1039/C3TA13335D.

[56] A. Orfanidi, M.K. Daletou, S.G. Neophytides, Mitigation strategy towards stabilizing the electrochemical interface under high CO and H_2O containing reformate gas feed, Electrochim. Acta 233 (2017) 218–228, https://doi.org/10.1016/j.electacta.2017.03.013.

[57] K.J.J. Mayrhofer, D. Strmcnik, B.B. Blizanac, V. Stamenkovic, M. Arenz, N.M. Markovic, Measurement of oxygen reduction activities via the rotating disc electrode method: from Pt model surfaces to carbon-supported high surface area catalysts, Electrochim. Acta 53 (2008) 3181–3188, https://doi.org/10.1016/j.electacta.2007.11.057.

[58] C. Roth, M. Goetz, H. Fuess, Synthesis and characterization of carbon-supported Pt–Ru–WOx catalysts by spectroscopic and diffraction methods, J. Appl. Electrochem. 31 (2001) 793–798, https://doi.org/10.1023/A:1017585901064.

[59] Y. Takasu, R. Unwin, B. Tesche, A.M. Bradshaw, Photoemission from palladium particle arrays on an amorphous silica substrate, Surf. Sci. 77 (1978) 219–232, https://doi.org/10.1016/0039-6028(78)90003-1.

[60] W. Eberhardt, P. Fayet, D.M. Cox, Z. Fu, A. Kaldor, R. Sherwood, D. Sondericker, Photoemission from mass-selected monodispersed Pt clusters, Phys. Rev. Lett. 64 (1990) 780–783, https://doi.org/10.1103/PhysRevLett.64.780.

[61] A.S. Aricò, V. Antonucci, N. Giordano, Methanol oxidation on carbon-supported platinum-tin electrodes in sulfuric acid, J. Power Sources 50 (1994) 295–309, https://doi.org/10.1016/0378-7753(94)01908-8.

[62] A.K. Shukla, M.K. Ravikumar, A. Roy, S.R. Barman, D.D. Sarma, A.S. Aricò, V. Antonucci, L. Pino, N. Giordano, Electro-oxidation of Methanol in Sulfuric Acid Electrolyte on Platinized-Carbon Electrodes with Several Functional-Group Characteristics, J. Electrochem. Soc. 141 (1994) 1517–1522, https://doi.org/10.1149/1.2054955.

[63] J.R. Croy, S. Mostafa, L. Hickman, H. Heinrich, B.R. Cuenya, Bimetallic Pt-Metal catalysts for the decomposition of methanol: effect of secondary metal on the oxidation state, activity, and selectivity of Pt, Appl. Catal. A Gen. 350 (2008) 207–216, https://doi.org/10.1016/j.apcata.2008.08.013.

[64] NIST X-ray Photoelectron Spectroscopy Database, Version 3.4 (Web Version), (2019) http://srdata.nist.gov/xps/index.htm.

[65] A.S. Arico, A.K. Shukla, H. Kim, S. Park, M. Min, V. Antonucci, An XPS study on oxidation states of Pt and its alloys with Co and Cr and its relevance to electroreduction of oxygen, Appl. Surf. Sci. 172 (2001) 33–40, https://doi.org/10.1016/S0169-4332(00)00831-X.

[66] M.K. Bayazit, L.S. Clarke, K.S. Coleman, N. Clarke, Pyridine-functionalized single-walled carbon nanotubes as gelators for poly(acrylic acid) hydrogels, J. Am. Chem. Soc. 132 (2010) 15814–15819, https://doi.org/10.1021/ja1076662.

[67] J. Agullo, M. Morin, D. Bélanger, Modification of glassy carbon electrode by electrografting of in situ generated 3-diazopyridinium cations, J. Electrochem. Soc. 159 (2012) H758–H764, https://doi.org/10.1149/2.054209jes.

[68] Y. Luo, N. Shroti, M.K. Daletou, L.A. Estudillo-Wonga, N. Alonso-Vante, Synergistic effect of Yttrium and pyridine-functionalized carbon nanotube on platinum nanoparticles toward the oxygen reduction reaction in acid medium, J. Catal. 344 (2016) 712–721, https://doi.org/10.1016/j.jcat.2016.09.014.

[69] H. Yoshida, Y. Yazawa, N. Takagi, A. Satsuma, T. Tanaka, S. Yoshida, T. Hattori, XANES study of the support effect on the state of platinum catalysts, J. Synchrotron Rad. 6 (1999) 471–473, https://doi.org/10.1107/S0909049598017919.

[70] S. Mukerjee, J. McBreen, Effect of particle size on the electrocatalysis by carbon-supported Pt electrocatalysts: an in situ XAS investigation, J. Electroanal. Chem. Lausanne (Lausanne) 448 (1998) 163–171, https://doi.org/10.1016/S0022-0728(97)00018-1.

[71] M. Steffan, F. Klasovsky, J. Arras, C. Roth, J. Radnik, H. Hofmeister, P. Claus, Carbon-Carbon Double Bond versus Carbonyl Group Hydrogenation: Controlling the Intramolecular Selectivity with Polyaniline-Supported Platinum Catalysts, Adv. Synth. Catal. 350 (2008) 1337–1348, https://doi.org/10.1002/adsc.200800035.

[72] A. Katrib, The reduction of Pt(IV) to Pt(II) by X-ray and argon-ion bombardment; evidence from X-ray photoelectron spectroscopy, J. Electron Spectrosc. Relat. Phenom. 18 (1980) 275–278, https://doi.org/10.1016/0368-2048(80)80054-5.

[73] A.V. Kalinkin, M.Y. Smirnov, A.I. Nizovskii, V.I. Bukhtiyarov, X-ray photoelectron spectra of platinum compounds excited with monochromatic AgLα irradiation, J. Electron Spectrosc. Relat. Phenom. 177 (2010) 15–18, https://doi.org/10.1016/j.elspec.2009.09.007.

[74] H.E. van Dam, H. van Bekkum, Preparation of platinum on activated carbon, J. Catal. 131 (1991) 335–349, https://doi.org/10.1016/0021-9517(91)90269-A.

[75] H.C. Choi, M. Shim, S. Bangsaruntip, H. Dai, Spontaneous reduction of metal ions on the sidewalls of carbon nanotubes, J. Am. Chem. Soc. 124 (2002) 9058–9059, https://doi.org/10.1021/ja026824t.

[76] M. Wojnicki, K. Paclawski, R.P. Socha, K. Fitzner, Adsorption and reduction of platinum(IV) chloride complex ions on activated carbon, Trans. Nonferrous Met. Soc. China 23 (2013) 1147–1156, https://doi.org/10.1016/S1003-6326(13)62577-7.

[77] C. Leon, Y. Leon, J. Solar, V. Calemma, L. Radovic, Evidence for the protonation of basal plane sites on carbon, Carbon 30 (1992) 797–811, https://doi.org/10.1016/0008-6223(92)90164-R.

[78] J. Lambert, M. Che, The molecular approach to supported catalysts synthesis: state of the art and future challenges, J. Mol. Catal. A Chem. 162 (2000) 5–18, https://doi.org/10.1016/S1381-1169(00)00318-6.

[79] K. Shinozaki, J.W. Zack, R.M. Richards, B.S. Pivovar, S.S. Kocha, Oxygen Reduction Reaction Measurements on platinum electrocatalysts utilizing Rotating Disk

Electrode technique. I. Impact of impurities, measurement protocols and applied corrections, J. Electrochem. Soc. 162 (2015) F1144–F1158, https://doi.org/10.1149/2.1071509jes.
[80] K. Shinozaki, J.W. Zack, S. Pylypenko, B.S. Pivovar, S.S. Kocha, Oxygen Reduction Reaction measurements on platinum electrocatalysts utilizing Rotating Disk Electrode technique. II. Influence of ink formulation, catalyst layer uniformity and thickness, J. Electrochem. Soc. 162 (2015) F1384–F1396, https://doi.org/10.1149/2.0551512jes.
[81] U.A. Paulus, T.J. Schmidt, H.A. Gasteiger, R.J. Behm, Oxygen reduction on a high-surface area Pt/Vulcan carbon catalyst: a thin-film rotating ring-disk electrode study, J. Electroanal. Chem. Lausanne (Lausanne) 495 (2001) 134–145, https://doi.org/10.1016/s0022-0728(00)00407-1.
[82] E. Higuchi, H. Uchida, M. Watanabe, Effect of loading level in platinum-dispersed carbon black electrocatalysts on oxygen reduction activity evaluated by rotating disk electrode, J. Electroanal. Chem. Lausanne (Lausanne) 583 (2005) 69–76, https://doi.org/10.1016/j.jelechem.2005.01.041.
[83] J. Schmidt, H.A. Gasteiger, G.D. Stab, P.M. Urban, D.M. KoIb, R.J. Behm, Characterization of high-surface-area electrocatalysts using a Rotating Disk Electrode configuration, J. Electrochem. Soc. 145 (1998) 2354–2358, https://doi.org/10.1149/1.1838642.
[84] Y. Garsany, O.A. Baturina, K.E. Swider-Lyons, S.S. Kocha, Experimental methods for quantifying the activity of platinum electrocatalysts for the oxygen reduction reaction, Anal. Chem. 82 (2010) 6321–6328, https://doi.org/10.1021/ac100306c.
[85] H. Yang, S. Kumar, S. Zou, Electroreduction of O2 on uniform arrays of Pt nanoparticles, J. Electroanal. Chem. Lausanne (Lausanne) 688 (2013) 180–188, https://doi.org/10.1016/j.jelechem.2012.08.030.
[86] M. Nesselberger, M. Roezfaad, R. Fayçal Hamou, P.U. Biedermann, F. Schweinberger, S. Kunz, K. Schloegl, G. Wiberg, S. Ashton, U. Heiz, K.J.J. Mayrhofer, M. Arenz, The effect of particle proximity on the oxygen reduction rate of size-selected platinum clusters, Nat. Mater. 12 (2013) 919–924, https://doi.org/10.1038/nmat3712.
[87] M. Inaba, H. Yamada, J. Tokunaga, A. Tasaka, Effect of agglomeration of Pt/C catalyst on hydrogen peroxide formation, Electrochem. Solid State Lett. 7 (2004) A474–A476, https://doi.org/10.1149/1.1814595.
[88] V. Stamenkovic, B.S. Mun, K.J.J. Mayrhofer, P.N. Ross, N.M. Markovic, J. Rossmeis, J. Greeley, J.K. Nørskov, Changing the activity of electrocatalysts for Oxygen Reduction by tuning the surface electronic structure, Angew. Chem.-Int. Ed. 45 (2006) 2897–2901, https://doi.org/10.1002/anie.200504386.
[89] B. Hammer, J. Nørskov, Theoretical surface science and catalysis-calculations and concepts, J. Adv. Catal. Sci. Technol. 45 (2000) 71–129, https://doi.org/10.1016/S0360-0564(02)45013-4.
[90] Y. Takasu, N. Ohashi, X.-G. Zhang, Y. Murakami, H. Minagawa, S. Sato, K. Yahikozawa, Size effects of platinum particles on the electroreduction of oxygen, Electrochim. Acta 41 (1996) 2595–2600, https://doi.org/10.1016/0013-4686(96)00081-3.
[91] K.J.J. Mayrhofer, B.B. Blizanac, M. Arenz, V.R. Stamenkovic, P.N. Ross, N.M. Markovic, The impact of geometric and surface electronic properties of Pt-Catalysts on the particle size effect in electrocatalysis, J. Phys. Chem. B 109 (2005) 14433–14440, https://doi.org/10.1021/jp051735z.
[92] H. Yang, S. Kumar, S. Zou, Electroreduction of O_2 on uniform arrays of Pt nanoparticles, J. Electroanal. Chem. Lausanne (Lausanne) 688 (2013) 180–188, https://doi.org/10.1016/j.jelechem.2012.08.030.